AD NUMBER

B197 442

NEW LIMITATION CHANGE

TO Approved for Public Release;
Distribution Unlimited.
** Stmt: A
** Code: 1

FROM

N/A

AUTHORITY

DTIC-D, thru Chief, DTIC-OCC - 95ØS31

SACLANTCEN REPORT
serial no.: SR-226

SACLANT UNDERSEA RESEARCH CENTRE

REPORT

Three-dimensional distribution of sound speed in the Iceland–Faeroe area, retrieved from a CTD survey, thermistor-chain measurements and satellite SST imagery

H.-H. Essen and
J. Sellschopp

November 1994

The SACLANT Undersea Research Centre provides the Supreme Allied Commander Atlantic (SACLANT) with scientific and technical assistance under the terms of its NATO charter, which entered into force on 1 February 1963. Without prejudice to this main task – and under the policy direction of SACLANT – the Centre also renders scientific and technical assistance to the individual NATO nations.

Page count for SR-226 (excluding Covers and Data Sheet)

Pages	Total
i–vi	6
1–40	40
	46

SACLANT Undersea Research Centre
Viale San Bartolomeo 400
19138 San Bartolomeo (SP), Italy

tel: 0187 540 111
fax: 0187 524 600
telex: 271148 SACENT I

NORTH ATLANTIC TREATY ORGANIZATION

SACLANTCEN SR-226

Three-dimensional distribution of sound speed in the Iceland–Faeroe area, retrieved from a CTD survey, thermistor-chain measurements and satellite SST imagery

H.-H. Essen and J. Sellschopp

The content of this document pertains to work performed under Project 23 of the SACLANTCEN Programme of Work. The document has been approved for release by The Director, SACLANTCEN.

David L. Bradley
Director

intentionally blank page

Three-dimensional distribution of sound speed in the Iceland–Faeroe area, retrieved from a CTD survey, thermistor-chain measurements and satellite SST imagery

H.-H. Essen and J. Sellschopp

Executive Summary: As a result of the political changes of recent years, regions of military threat are no longer well defined. For this reason the possibility of rapidly assessing unknown areas has gained importance. Obviously, satellite remote sensing is one appropriate tool for this purpose. Large areas of the ocean may be observed synoptically, but unfortunately, satellite-borne instruments can only view the sea surface and this information is of little help in, for example, the prediction of sonar performance. For this purpose sophisticated mathematical models exist, the utility of which is mainly restricted by an insufficient knowledge of environmental parameters. Information on the boundaries –sea surface and seafloor– is required, and for the inner ocean, the dependence of sound speed on all three spatial coordinates.

This report develops methods to extract subsurface sound speed from satellite-measured surface temperatures (SSTs), which of course need some *a priori* information on the area under consideration. The satellite data are from the advanced very high resolution radiometer (AVHRR) of the series of NOAA satellites. Subsurface sound speeds are taken from investigations in the Iceland–Faeroe Frontal (IFF) region, where in 1989, besides vertical profiles at selected positions (SACLANTCEN), profiles from a towed thermistor-chain (FWG, Germany) were also available. The methods used here are based on the decomposition of the vertical sound-speed profiles in so-called empirical orthogonal eigenfunctions (EOFs). As is known from the Gulf Stream area most of the sound-speed variance can be well represented by a small number of EOFs. By making use of the subsurface data of both sources, this report proves that the decomposition into EOFs is also possible for the oceanographically complex IFF area. The first three EOFs account for 98% of the sound-speed variance. Thus, the amplitudes of these EOFs, as a function of range, represent the three-dimensional sound-speed distribution.

By means of a correlation analysis it has been found that only the amplitude of the first EOF can be derived from SST, which may be measured from space. Already, the first EOF contains important information on the subsurface sound speed, mainly on the long-scale variability. Changes of sound-speed profiles across meandering thermal fronts and within eddies may be determined, but, compared to the thermistor-chain measurements, the reconstructed sound-speed distribution is considerably smoothed. In order to overcome this problem, for the purpose of acoustic modelling, a theoretical model, based on the EOF decomposition, has been constructed. Random EOF amplitudes have been synthesized in accordance with the statistical properties of the satellite-measured SSTs. The modelled vertical sound-speed distribution provides a good representation of the features of the measured data.

This report shows that important features of the subsurface sound speed may be derived from satellite-measured SSTs. Crucial for the methods described is a knowledge of the EOFs and the degree of correlation between their amplitudes and SST. In the future, oceanographic research at SACLANTCEN will concentrate on shallow-water coastal areas of the Mediterranean. The methods derived in this report will be tested to determine if they are also applicable in these regions. In order to resolve the small-scale variability, chain measurements are required.

Three-dimensional distribution of sound speed in the Iceland–Faeroe area, retrieved from a CTD survey, thermistor-chain measurements and satellite SST imagery

H.-H. Essen and J. Sellschopp

Abstract: The three-dimensional variability of sound speed in the Iceland-Faeroe Frontal (IFF) region is investigated. Emphasis is put on the question, to what extend subsurface sound speed may be determined from spaceborne remote sensing. Data from different sources are used: CTD survey and thermistor-chain measurements as ground truth and satellite infrared imagery. Most of the data are temperatures which, for the area under consideration, quite accurately determine the sound speed. From the subsurface data it is shown that the vertical sound-speed profiles can be decomposed into empirical orthogonal eigenfunctions (EOFs), with the first two already accounting for 97% of the variance. High correlation of the first- and second-order EOF amplitudes is found with sea-surface dynamic height, and for the first-order EOF amplitude with sea-surface temperature (SST). The latter relation is used successfully to determine subsurface sound speeds from satellite-measured SSTs. Due to the resolution of the satellite data, horizontal scales are overestimated, and due to the availability of only the first-order EOF amplitude for the construction of sound-speed profiles, a too high vertical correlation is introduced. To overcome these problems, for the purpose of acoustic modelling, a theoretical three-dimensional sound-speed model is developed, based on the EOF decomposition. The EOF amplitudes contain the analytically described front and random portions represented by a finite moving average process.

Keywords: CTD survey ○ Iceland-Faeroe Front ○ satellite infrared imagery ○ sound-speed variability ○ thermistor chain

Contents

Acknowledgements: Thanks go to the crews of R/V *Alliance* and R/V *Planet*. The CTD data were collected and processed by the Ocean Engineering Department (OED) and Applied Oceanography Group (AOG) at SACLANTCEN. The thermistor-chain data are from FWG (Germany). E. Nacini from SACLANTCEN processed the AVHRR image.

1
Introduction

Sound propagation is determined by the spatial variability of the 'frozen' ocean. A quasi-synoptic view of the ocean is only available from satellite imagery, e.g., sea-surface temperatures (SST) from infrared imagery. Unfortunately, satellite measurements are restricted to the sea surface and provide no direct subsurface information, which is mainly needed for the purpose mentioned. Subsurface data used in this report are from a CTD survey carried out by SACLANTCEN from onboard R/V *Alliance* and thermistor-chain measurements performed by FWG with R/V *Planet*. Because of the time involved both data sets contain, beside the spatial variability, temporal influences from e.g. internal waves or tides. To some extent, these influences distort the spatial information. For our investigation we ignore this problem but keep in mind that it may be a cause of error. Most of the data are temperatures which, for the area under consideration, quite accurately determine the sound speed. Both CTD and thermistor-chain data contain the vertical sound-speed variability. While the CTD data extend to greater depths, they do not resolve the horizontal scales. The thermistor-chain also yields high resolution in one horizontal dimension (along track). Information on the two-dimensional horizontal variability with high resolution is only available from satellite images of the sea surface. SST has been recorded by space-borne infrared radiometers for some fifteen years from onboard the series of NOAA satellites. Retrieval algorithms for the advanced very high resolution radiometer (AVHRR) have been developed at SACLANTCEN and applied mainly to data from the Iceland-Faeroe Frontal (IFF) region. The main disadvantage of radiometry for oceanographic investigations is the requirement for a cloud-free sky. Especially in the IFF region, SACLANTCEN's area of interest during recent years, this restriction is of considerable importance. Only a small number of unperturbed images are available, which do not allow to study the temporal evolution of oceanographic phenomena to be studied.

The sound-speed distribution in the IFF area is characterized by the presence of a front, which separates warm Atlantic and cold Arctic water masses and extends from Iceland to north of the Faeroe Islands following the topography. Water depths vary from more than 2000 m on both sides of the Iceland-Faeroe Ridge to less than 400 m on the ridge itself. The area is characterized by occasional excursions of the front to the north of some 100 km, with meanders and eddies. In general, temperature gradients are steeper close to Iceland than in the eastern part of the front. A review of the physical oceanography of this region is given by Hopkins (1988). From both CTD and thermistor-chain data, the sound speed is obtained as a function of depth. It is shown that for the IFF region the vertical sound-speed profiles can be decomposed into empirical orthogonal eigenfunctions (EOFs) with the first two

EOFs accounting for the major part of the variance. Recent investigations from the Gulf Stream area showed a strong correlation between first- and second-order EOF amplitudes and dynamic height. Dynamic height is a feature of the sea surface and can be recorded by satellite altimetry. In principle, this opens the possibility of observing, from space, the subsurface variability of sound speed. For the IFF area, similar correlations have been found. But the variability of dynamic height is less than in the Gulf Stream and with ± 10 cm just about the same as the accuracy of presently operating altimeters. With respect to SST, high correlation has been found only for the first-order EOF amplitudes.

Section 2 of this report presents the data, which are from a CTD survey, a towed thermistor-chain, and an AVHRR (channel 4) image. Methods of analysis are described in Sect. 3. Vertical sound-speed profiles, as derived from the CTD and thermistor-chain data are decomposed into EOFs. The horizontal variability is accounted for by means of the statistical descriptors autocorrelation function and variance spectrum. Sect. 4 investigates the correlation between EOF amplitudes and both dynamic height and SST. Subsurface sound-speed profiles are constructed from satellite measured SSTs. Using both the vertical decomposition into EOFs and the information on horizontal scales, a synthetic model of the three-dimensional sound-speed distribution is developed in Sect. 5.

2
Data

The purpose of this report is to determine the distribution of sound speed, which depends on temperature, salinity and water depth by (cf. Brekhovskikh and Lysanov, 1991),

$$c = 1449.2 + 4.6T - 0.055T^2 + 0.00029T^3 + (1.34 - 0.01T)(S - 35) + 0.016D, \quad (1)$$

where c [ms^{-1}] is the sound speed, T [°C] the temperature, S [ppt] the salinity and D [m] the depth. Only one of the data sources (CTD survey) considered yields all the data required by (1). Fortunately, salinity has less influence on sound speed than temperature and depth. At least, this is true for the strong variations across the main front in the IFF region. Here, temperatures deviate by ±3°C from the mean, causing sound-speed variations of ±12 ms^{-1}, while the variations due to salinity are less than 1 ms^{-1} and may be ignored. Inserting the approximate salinity of 35 ppt and expanding the remaining equation around the temperature of 5°, we obtain,

$$c = 1450.5 + 4.07T + 0.016D. \quad (2)$$

For the data from the thermistor chain and the satellite this formula is used to derive the sound speed. The comparison of accurate sound speeds from CTD profiles with those derived by means of (2) yields excellent agreement.

2.1. CTD SURVEY

During various cruises from 1988 to 1993, CTD sections were carried out from on-board R/V *Alliance* in the IFF region. From these measurements, profiles of temperature (T), salinity (S), sound speed (c) and density (ρ) are available with 1 m sampling, starting 1 m below the sea surface down to some 50 m above the seafloor or to maximum of 2000 m if the water depth exceeds this value. The density referred to is in terms of $\sigma_t = \rho(T, S, p = 0)$. In order to reduce the amount of data, the profiles are averaged to 10 m intervals centred at 5.5 m, 15.5 m, etc. Occasionally, due to rough sea conditions, data are lacking for the uppermost 1–3 m. This only moves the centre of the first averaging interval but should have no influence on the analysis performed. In this report, we analyse data taken during a cruise from 8 to 21 June 1989. Figure 1 shows the locations of the CTD stations and the bathymetry of the area. Figure 2 displays all available ($N = 63$) vertical profiles of temperature, salinity, sound speed and density down to a maximum depth of 2000 m. Profiles not reaching this depth end about 50 m above the seafloor.

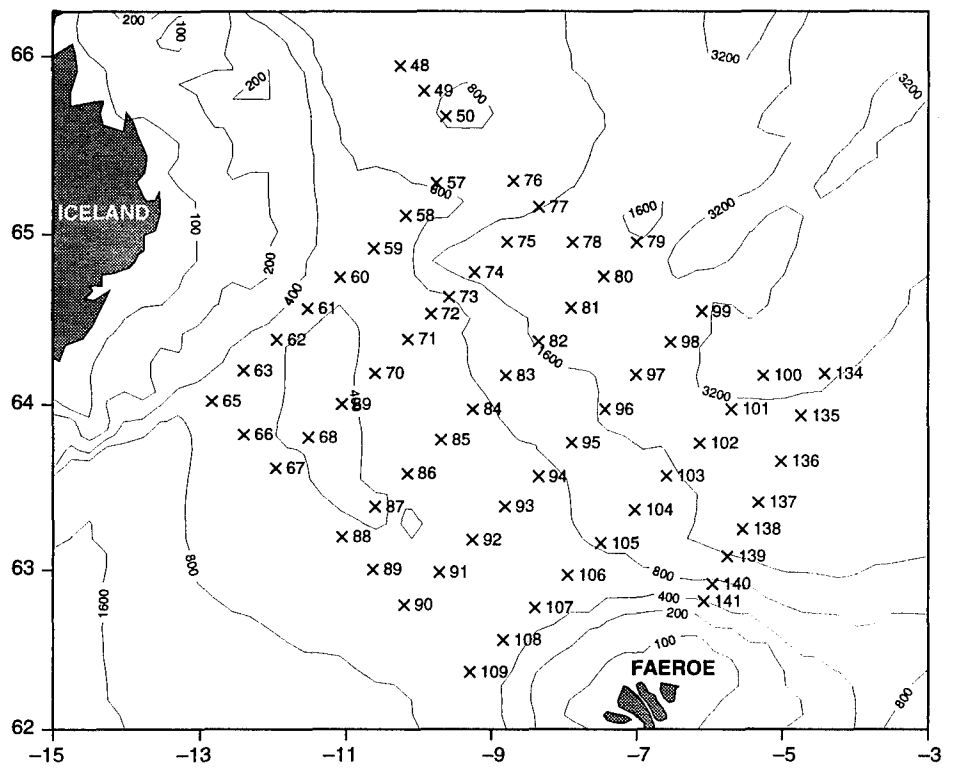

Figure 1 *CTD stations during R/V Alliance cruise 8–21 June 1989, together with bathymetry of the area.*

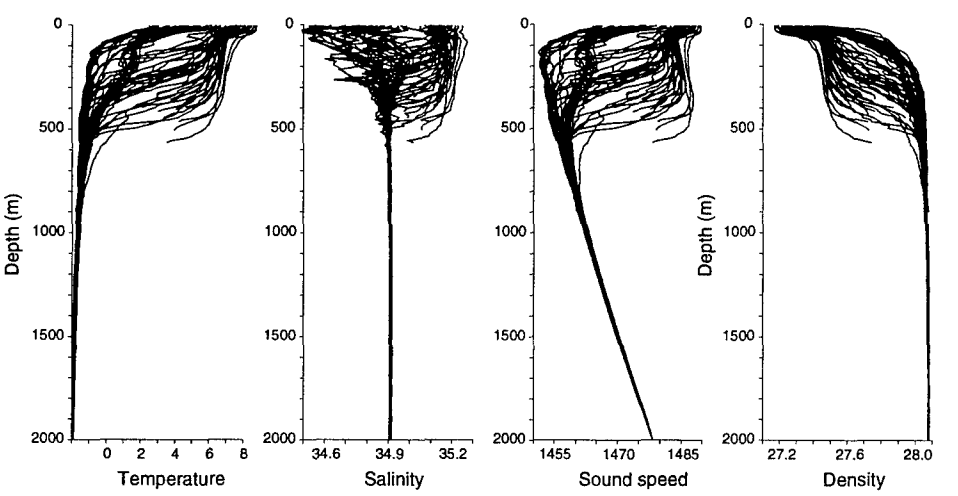

Figure 2 *Vertical profiles of temperature [°C], salinity [ppt], sound speed [ms^{-1}], density in terms of σ_t [kg m^{-3}] of all stations shown in Fig. 1.*

2.2. THERMISTOR-CHAIN DATA

The data investigated here are from a cruise of R/V *Planet* to the IFF area in summer 1989. The 200 m chain contains 60 thermistors at 3 m spacing (Sellschopp, 1987). The accuracy of the thermistors is better than 0.05°C with a time constant of about 40 s. Data were sampled every 12 s. No pressure sensors were incorporated in the chain cable used in this experiment. The angle between the upper part of the cable and the vertical axis at towing speeds around 3 ms^{-1} is about 40° and becomes smaller at the lower end. An approximate estimation of the sensor depth D in m is

$$D = 15.0 + 2.25 \times (l - 1), \tag{3}$$

where $l = 1, \ldots, 60$ is the sensor number. Positions of the ship are available every half hour from the bridge report. Thus, both the vertical and horizontal positions of the thermistors can be determined with only limited accuracy.

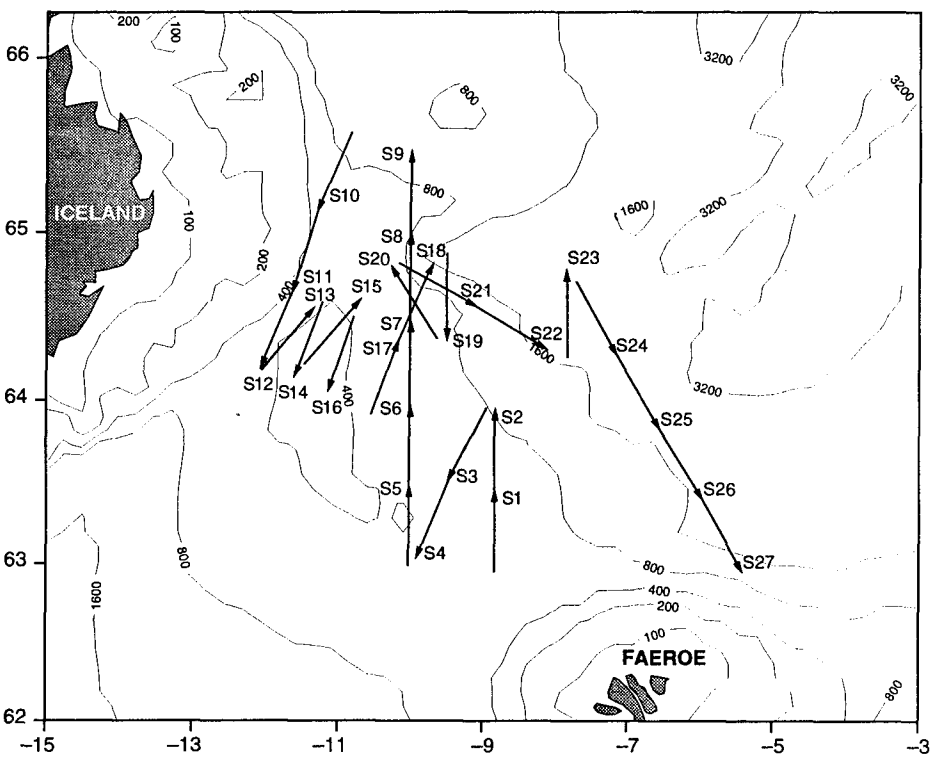

Figure 3 *Thermistor-chain sections of the R/V Planet from 8–15 July 1989, together with bathymetry of the area.*

From the data available, 27 sections have been selected under the constraints that they should extend to at least 50 km and the ship's course and speed should be relatively constant (as determined from the ship's positions). The sections are presented in Fig. 3. Table 1 contains some of the parameters for these sections: starting time,

length, mean speed and course of the ship. Because of the relative low ship speed and the resultant uncertainty in depth, sections S10 and S11 have not been considered in the following analysis. The number of data has been reduced by sorting into depth intervals of 4.5 m, each containing 2 thermistors, cf. (3), and range intervals of 0.5 km, which have been determined by the measuring time and the ship's mean speed. Figures 4a–d present sound speeds from 4 selected sections (out of 27), as measured at the different depth levels (upper panel) and each second sound-speed profile, spaced by 1 km (lower panel). The sections are of somewhat different length (cf. Table 1), but only the first 50 km are displayed in order to allow for better comparison. The data of Figs. 4a–d are from south (Atlantic water) and north (Arctic water) of the front, sects. S5 and S9, respectively. Obviously, there is a higher spatial variability north of the front than south of it. In sect. S19 (Fig. 4c) the ship moved from north to south and passed the main front, which shows only little inclination against the vertical. Section S21 (Fig. 4d) is about parallel to the front and contains relatively high variability, with maximum amplitudes at depths around 50 m.

Table 1 *Specifications for the profiles in Fig. 3.*

Section	Starting time (UTC)	Duration (h)	Length (km)	Speed (ms^{-1})	Course (deg)
S 1	8-Jul-89 1:00	4.5	56.1	3.5	0
S 2	8-Jul-89 5:30	4.5	55.0	3.4	0
S 3	8-Jul-89 12:30	4.0	53.6	3.7	208
S 4	8-Jul-89 16:30	4.0	57.3	4.0	202
S 5	8-Jul-89 21:30	4.5	54.3	3.3	1
S 6	9-Jul-89 2:00	4.5	53.7	3.3	0
S 7	9-Jul-89 6:30	4.5	56.1	3.5	0
S 8	9-Jul-89 11:00	4.5	57.6	3.6	0
S 9	9-Jul-89 15:30	4.5	53.8	3.3	0
S10	10-Jul-89 16:30	8.5	54.1	1.8	204
S11	11-Jul-89 1:00	7.0	55.9	2.2	196
S12	11-Jul-89 8:00	5.0	54.9	3.1	203
S13	11-Jul-89 13:30	4.5	56.5	3.5	40
S14	11-Jul-89 19:00	5.0	55.3	3.1	201
S15	12-Jul-89 1:00	5.0	56.7	3.2	41
S16	12-Jul-89 7:30	5.5	55.1	2.8	199
S17	12-Jul-89 22:00	4.5	54.6	3.4	20
S18	13-Jul-89 2:30	4.5	55.9	3.5	24
S19	13-Jul-89 11:00	5.0	57.8	3.2	180
S20	13-Jul-89 18:00	5.5	58.9	3.0	328
S21	14-Jul-89 1:00	5.0	57.9	3.2	119
S22	14-Jul-89 6:00	4.5	54.3	3.3	122
S23	14-Jul-89 12:30	5.5	58.0	2.9	0
S24	14-Jul-89 19:00	5.0	58.9	3.3	152
S25	15-Jul-89 0:00	5.0	57.5	3.2	150
S26	15-Jul-89 5:00	4.5	55.3	3.4	148
S27	15-Jul-89 9:30	4.5	56.6	3.5	151

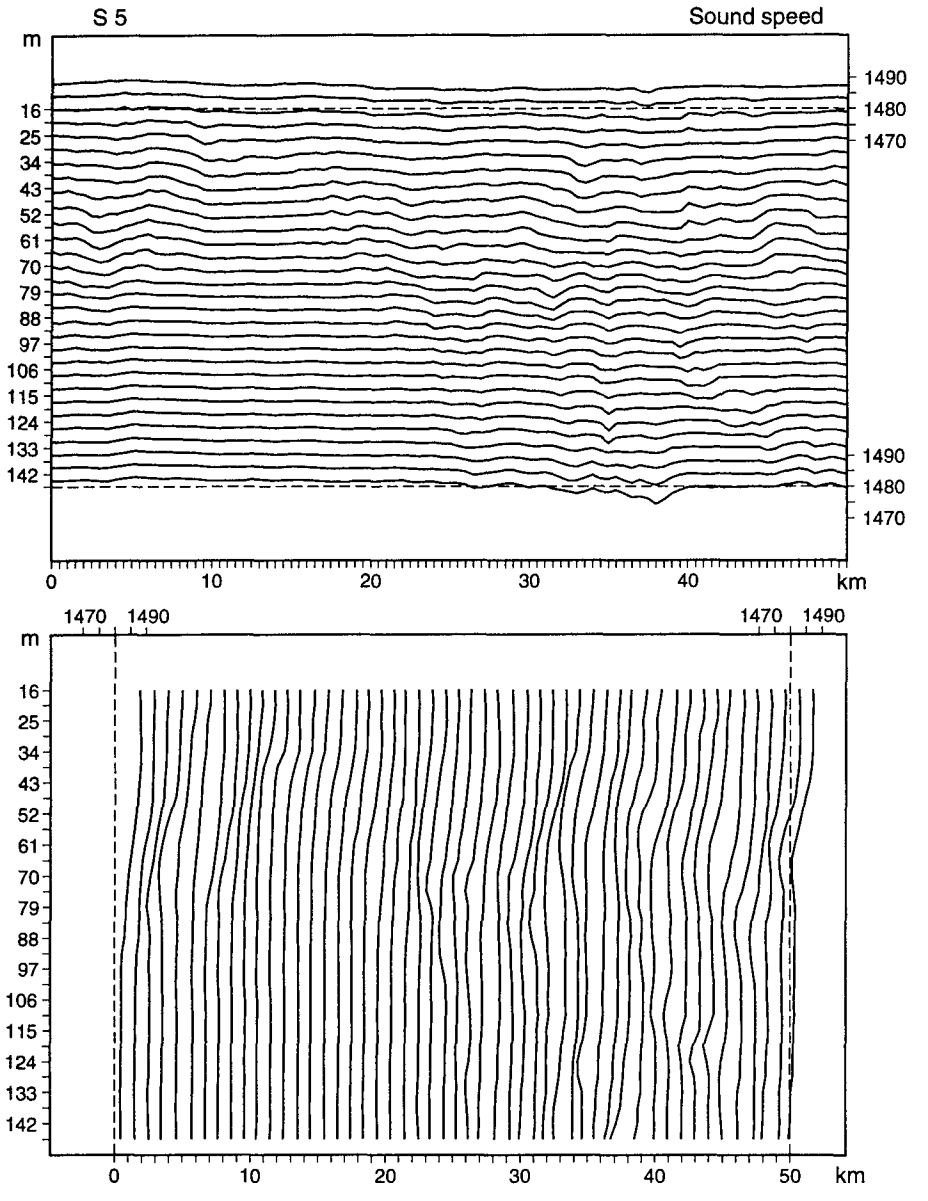

Figure 4a *Time series and vertical profiles of sound speed of section S5, (Fig. 3). The thermistor-chain data have been averaged vertically within 4.5 m and horizontally with 500 m intervals. Only each second vertical profile is displayed. Sound speed indicated are in* ms^{-1}. *The dashed lines refer to the uppermost and lowest depth level (upper panel) and the first and last profile (lower panel) of the section.*

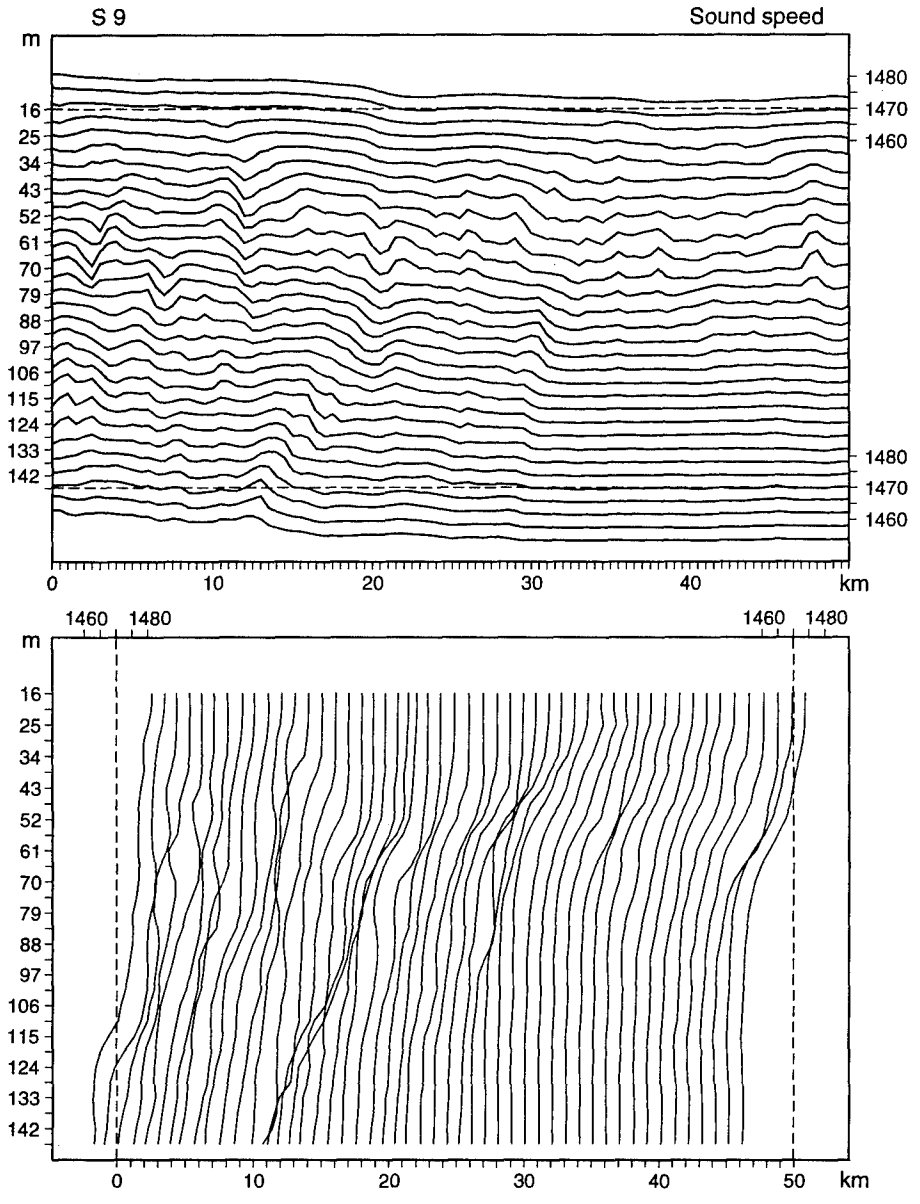

Figure 4b *Time series and vertical profiles of sound speed of section S9, (Fig. 3). The thermistor-chain data have been averaged vertically within 4.5 m and horizontally with 500 m intervals. Only each second vertical profile is displayed. Sound speed indicated are in* ms^{-1}. *The dashed lines refer to the uppermost and lowest depth level (upper panel) and the first and last profile (lower panel) of the section.*

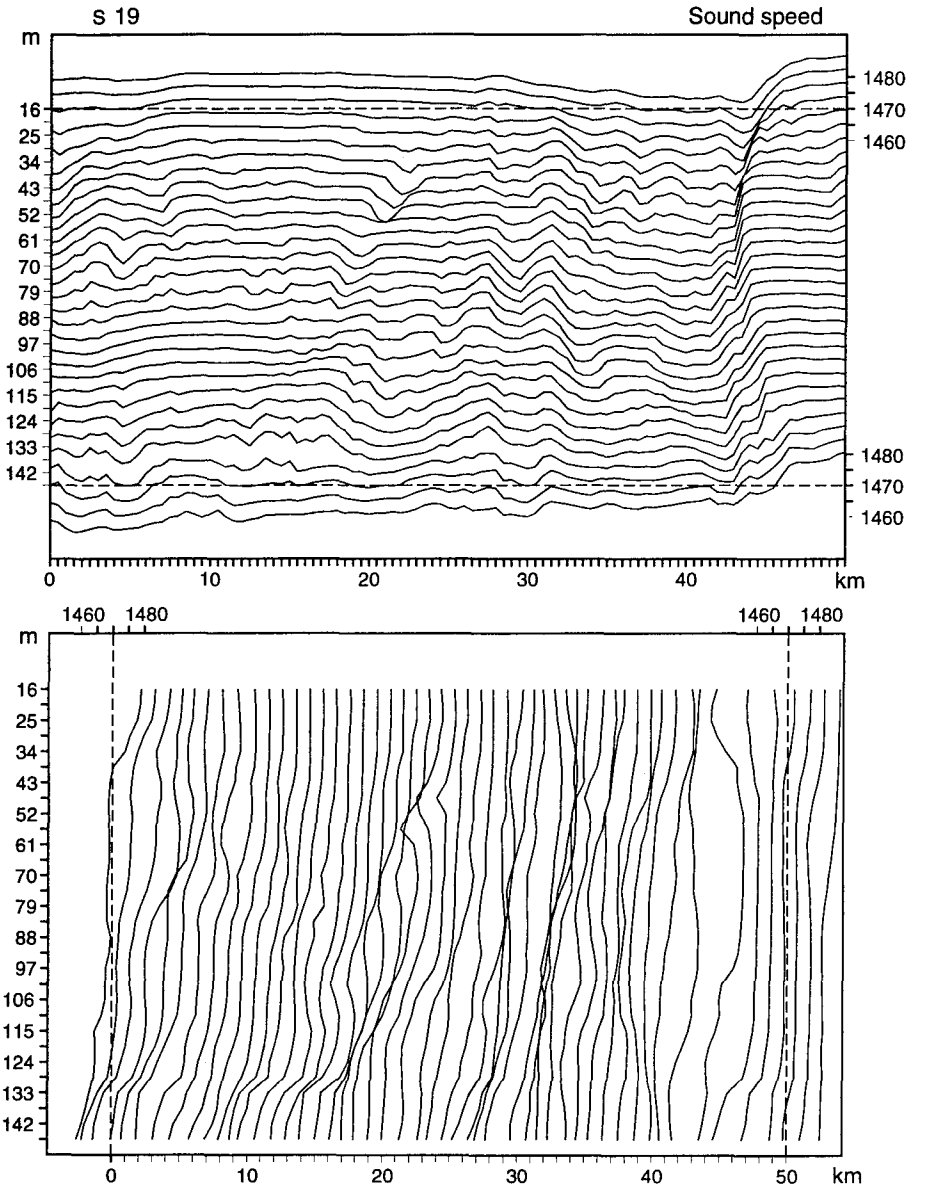

Figure 4c *Time series and vertical profiles of sound speed of section S19, (Fig. 3). The thermistor-chain data have been averaged vertically within 4.5 m and horizontally with 500 m intervals. Only each second vertical profile is displayed. Sound speed indicated are in* ms^{-1}. *The dashed lines refer to the uppermost and lowest depth level (upper panel) and the first and last profile (lower panel) of the section.*

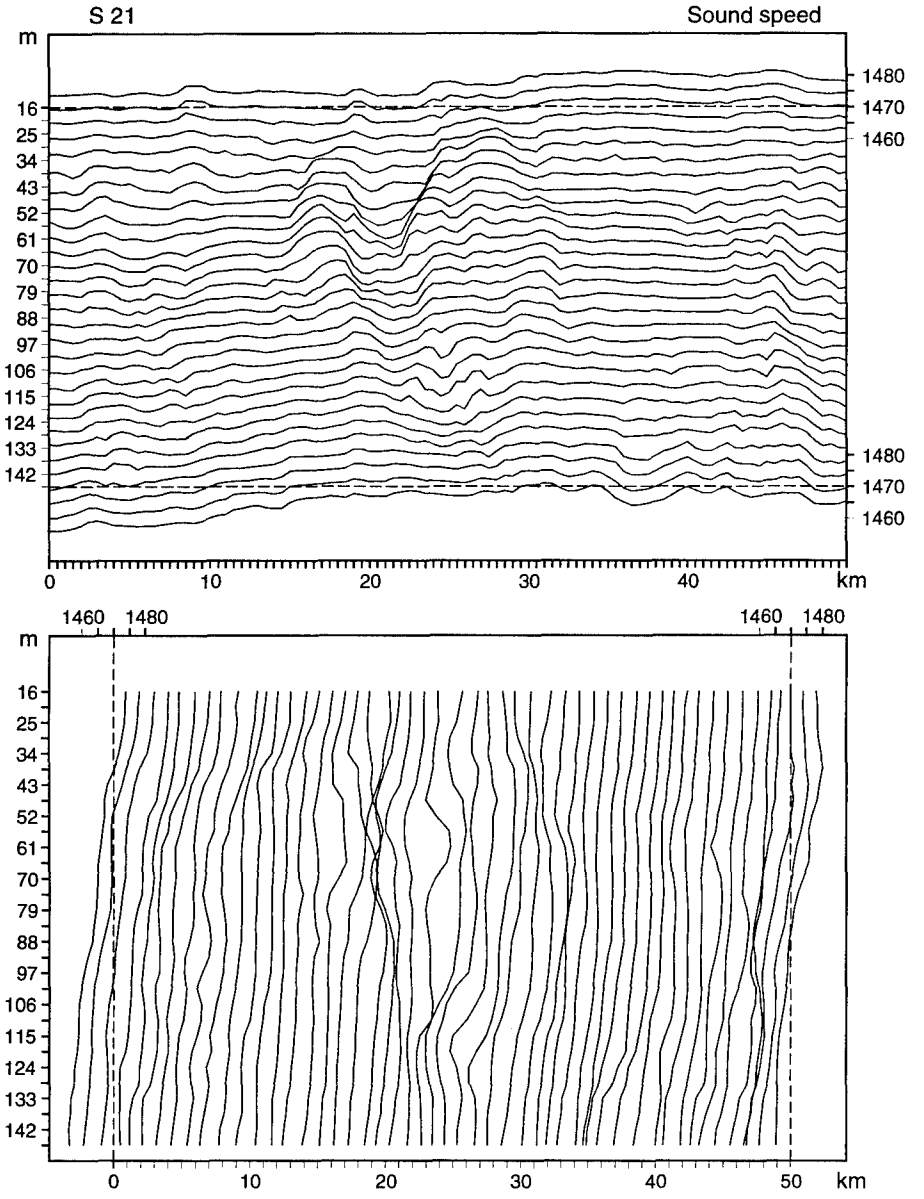

Figure 4d *Time series and vertical profiles of sound speed of section S21, (Fig. 3). The thermistor-chain data have been averaged vertically within 4.5 m and horizontally with 500 m intervals. Only each second vertical profile is displayed. Sound speed indicated are in* ms^{-1}. *The dashed lines refer to the uppermost and lowest depth level (upper panel) and the first and last profile (lower panel) of the section.*

2.3. SATELLITE SST IMAGES

Due to the nearly permanent cloud cover of the Iceland-Faeroe area, undisturbed satellite SST images are rare. Especially, for the investigation of small-scale variability a perfectly clear sky is required. Perturbation through clouds can lead to wrong conclusions. The example we use for our analysis is from 26 May 1989 and presented in Fig. 5. It is from the NOAA-10 satellite and displays the brightness temperatures of channel 4, which are different from the SST, usually a few degrees cooler, and the apparent SST variability is attenuated by about 10% (Minnett, 1991). Absolute temperatures may be derived by combining different infrared channels, but the mathematical procedures involved produce additional noise.

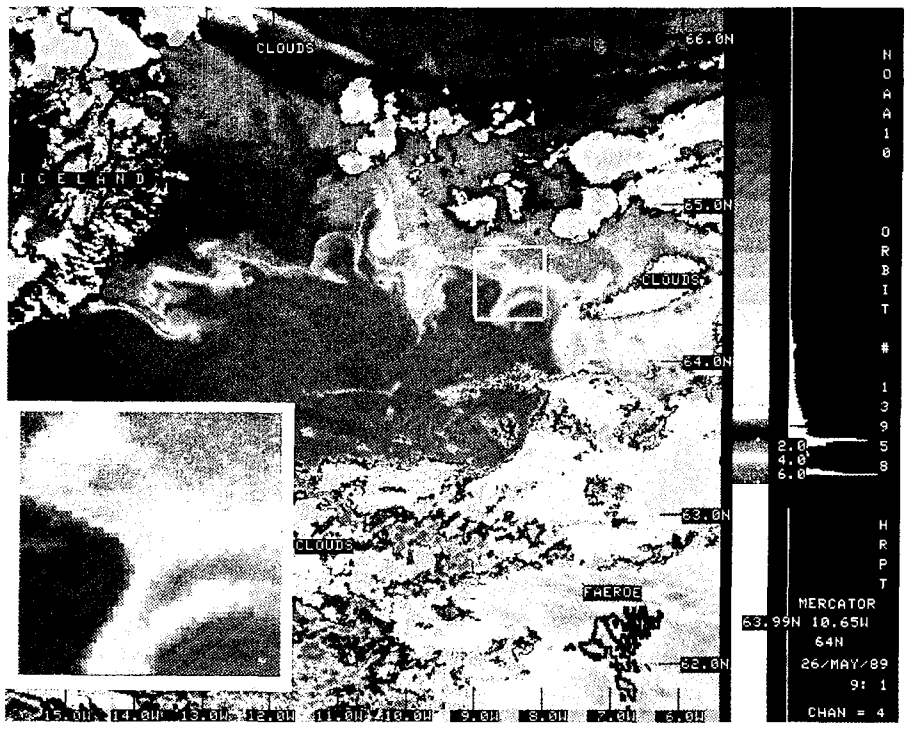

Figure 5 *Brightness temperatures [°C] measured by channel 4 of the AVHRR (NOAA-10) on 26 May 1989 in the Iceland-Faeroe frontal region.*

The frame in Fig. 5 indicates an area of 50 km × 50 km in the frontal zone. For this area sea-surface sound speeds have been computed by using (2) with $D = 0$ m. The gradients of the field describe the horizontal variability and eliminate the offset of the satellite against real SSTs. The vectors orthogonal to the gradients are more advantageous for representation,

$$\mathbf{u} = (-\frac{\mathrm{d}c}{\mathrm{d}y}, \frac{\mathrm{d}c}{\mathrm{d}x}), \tag{4}$$

and are displayed in Fig. 6. The satellite SSTs are given on a horizontal grid with about 1 km spacing in the IFF area. For Fig. 6 the data have been interpolated

onto a grid with 0.5 km spacing, from which the gradients are obtained by means of central differences. The purpose of this procedure is to emphasize the structure of variability, which in Sect. 5, will be compared with a synthetic model.

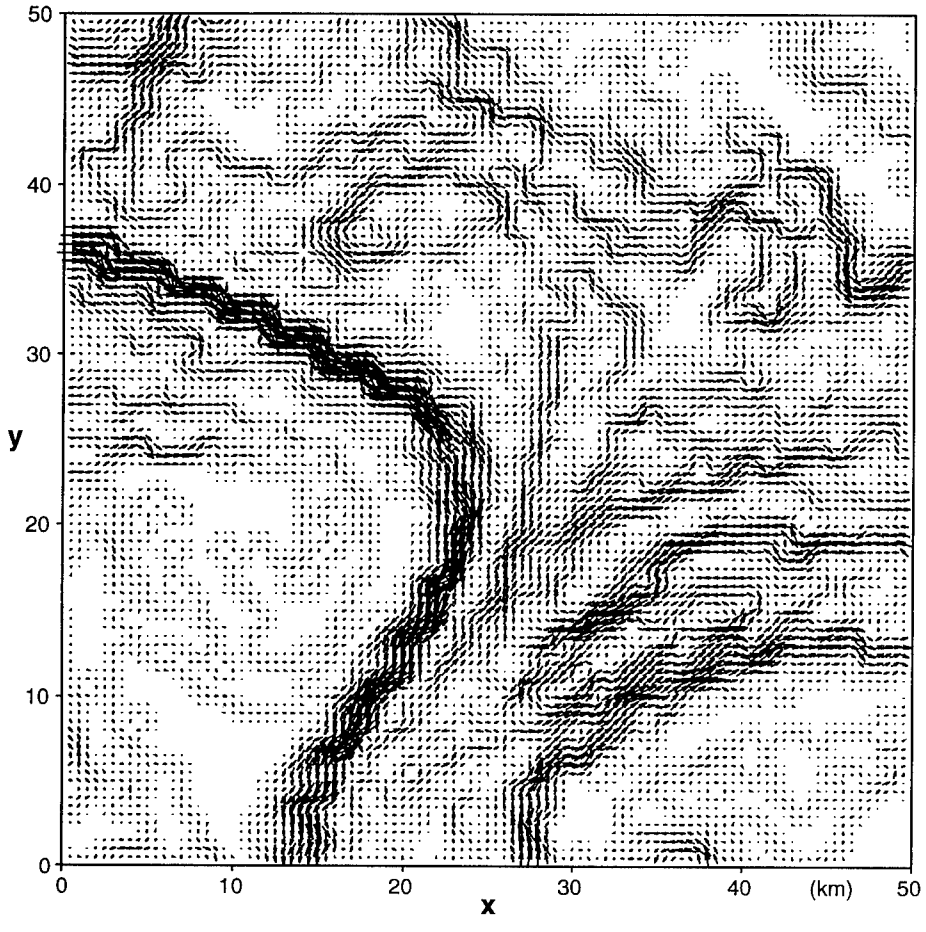

Figure 6 *Horizontal gradients of sound speed at the sea surface as derived from sea-surface temperatures in the frame of Fig. 5, represented by the orthogonal vectors (4). Coordinates point to the east (x-axis) and to the north (y-axis). Sound speeds of 1 km resolution are interpolated onto a grid with 0.5 km spacing. Gradients are computed via central differences.*

3
Data analysis

Both the CTD and thermistor-chain data describe the sound speed as a function of depth. It is well known that for selected areas vertical sound-speed profiles may be decomposed into a mean profile and two or three EOFs, which in general, account for more than 95% of the variance. For the horizontal variability we investigate the autocorrelation functions (ACF) and wavenumber variance spectra (WVS) of the thermistor-chain data and satellite images.

3.1. VERTICAL EOFS

The method of decomposing vertical sound-speed profiles into EOFs is briefly described. Considering L depth horizons, an $L \times L$-covariance matrix may be estimated by averaging over the profiles available,

$$R_{lk} = \frac{1}{N} \sum_{n=1}^{N} c_{ln} c_{kn}, \tag{5}$$

with

$$c_{ln} = C_{ln} - C_{l0}, \qquad C_{l0} = \frac{1}{N} \sum_{n=1}^{N} C_{ln}.$$

C_{ln} are the sound-speed profiles at locations $n = 1, \ldots, N$, with $l, k = 1, \ldots, L$ counting their depth horizons. C_{l0} is the mean profile. The EOFs are eigenvectors of the eigenvalue problem,

$$\sum_{k=1}^{L} R_{lk} e_k^{(m)} = \lambda^{(m)} e_l^{(m)}, \tag{6}$$

where $m = 1, \ldots, M = L$ are the mode numbers, $e_k^{(m)}$ are mutually orthogonal eigenfunctions (EOFs) and $\lambda^{(m)}$ are the eigenvalues. The sound-speed deviations (from the mean profile) may be decomposed into EOFs by

$$c_{ln} = \sum_{m=1}^{M} a_n^{(m)} e_l^{(m)}, \qquad a_n^{(m)} = \sum_{l=1}^{L} c_{ln} e_l^{(m)}. \tag{7}$$

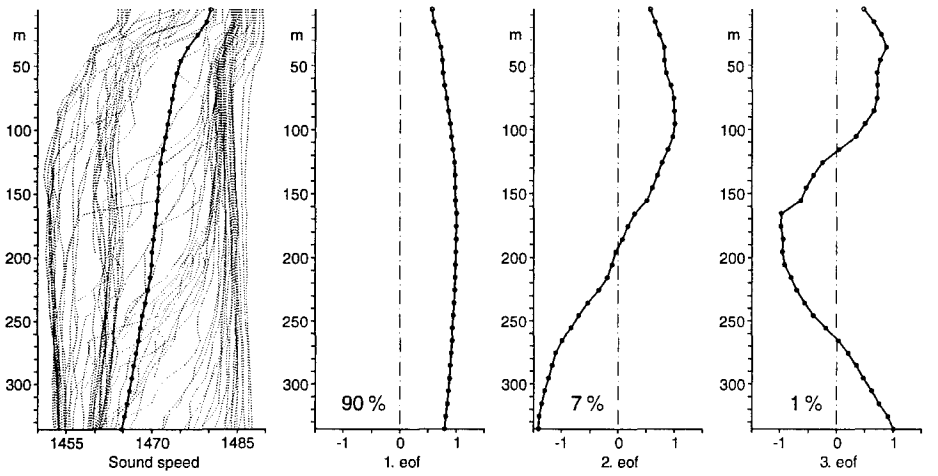

Figure 7 *Vertical sound-speed profiles from the CTD survey, and the first three EOFs. Dotted lines are the measured profiles, the full line (marked by circles) is the mean profile (left panel). Sound speeds are in* ms^{-1}. *The EOFs are arbitrarily normalised, their percentage amount of variance is indicated.*

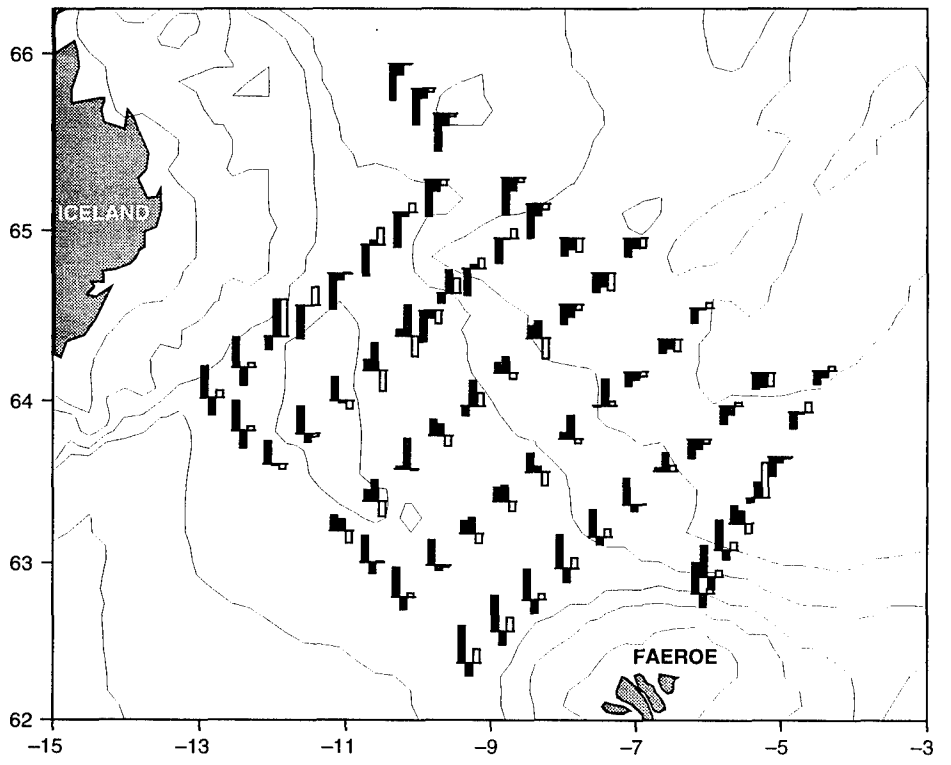

Figure 8 *Distribution of the EOF amplitudes from the CTD survey. first, second, and third EOF are represented by black, shaded and open columns, repectively. The amplitudes are arbitrarily normalised, separately for each EOF.*

The eigenvalues $\lambda^{(m)}$ describe the amount of variance as explained by the respective mode. Normally, a small number of modes contains most of the variance and summation over m in (7) may be restricted to values considerably smaller than L, i.e., $M \ll L$. In order to make use of all profiles available from the CTD survey, a maximum depth of 340 m has been chosen for the EOF analysis. Figure 7 (left) displays the sound-speed profiles (dotted lines) from the sea surface to this depth, together with the mean profile marked by circles. The first three EOFs are displayed and the amount of variance they account for is indicated, i.e., the first two EOFs account for 97% of the total variance. The first EOF shows only little vertical dependence and separates cold and warm water masses (see below), while the second and third EOFs describe vertical variability.

Figure 8 displays the distribution of the EOF amplitudes in the area of interest. The amplitudes are represented by black (first EOF), shaded (second EOF) and open (third EOF) columns. They are arbitrarily normalised, separately for each EOF. Obviously, first-order EOF amplitudes are attributed to the location with respect to the Iceland–Faeroe Ridge, which roughly coincides with the main front. Negative amplitudes are found north and positive amplitudes south of the front. A correlation with sea-surface temperatures can be expected and will be confirmed later. Second-order EOF amplitudes are positive in the vicinity of the front and become negative in more remote areas both north and south of the front. For the third-order amplitudes, no obvious relation to the front can be found, they show a more random distribution.

For four selected locations, Fig. 9 presents the reconstruction of measured sound-speed profiles by EOFs. The locations are from a section crossing the front from south to north, cf. Fig. 1. Solid lines with circles represent the measured sound speed. The dashed line is the mean profile, the three lines with increasing thickness represent the reconstruction with one, two, and three EOFs. South of the front (P69) the water is warmer than north of it (P75) and sound speeds are higher. Both these profiles are relatively smooth and may be well reconstructed by using only the first EOF. The two profiles in the frontal region (P71, P73) show higher vertical variability. A satisfactory reconstruction requires at least the first two EOFs.

Figure 10 displays the difference in sound speed between the measured and reconstructed profiles. Dotted, dashed and solid lines with circles refer to the reconstruction with one, two, and three EOFs, respectively. Though for some cases the reconstruction with only one EOF yields reasonable differences, a considerable improvement is found by adding the second EOF, while the consideration of the third EOF only affects a limited number of profiles. Computed from all data points available, the rms values of the sound-speed differences are 3.5 ms^{-1}, 1.7 ms^{-1}, and 1.1 ms^{-1} for reconstruction with one, two and three EOFs, respectively.

From the thermistor-chain measurements, sound-speed profiles have been constructed every 0.5 km along the sections listed in Table 1, except for S10 and S11. Though many of these 3000 profiles contain about the same information, all of them have

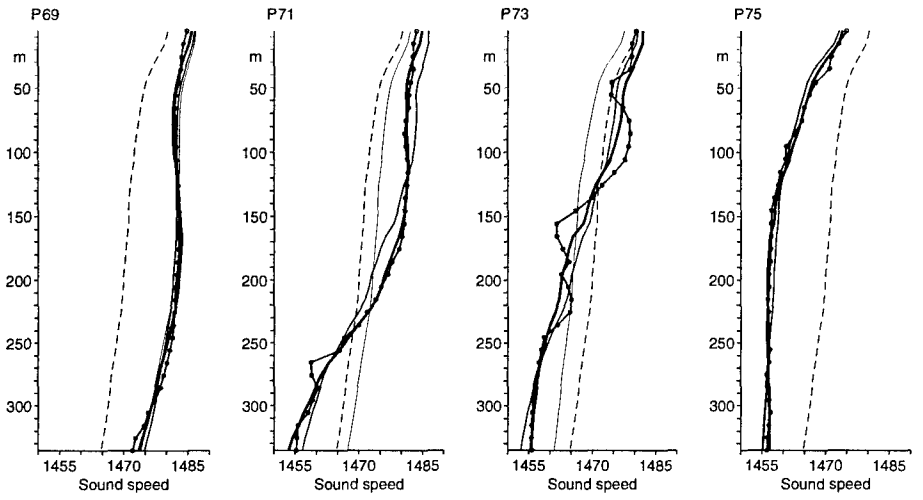

Figure 9 *Reconstruction of sound speed by means of EOFs for four chosen profiles of the CTD survey. Measured profiles (solid line with circles), mean profile (dashed line), and reconstructed profiles using one, two, and three EOFs (solid lines with increasing thickness) are displayed. Sound speeds are in* ms^{-1}.

been used for the EOF analysis. Figure 11 displays each 20th of the measured profiles and the mean profile (left panel: dotted lines and line marked by circles, respectively). In addition, Fig. 11 presents the first three EOFs with the amount of variance they account for indicated. For the first two EOFs this is 97%, which is the same value as found for the CTD survey, which extends to a greater depth.

Figure 12 shows the EOF amplitudes as a function of range for the sections of Table 1. From the section of different lengths (between 50 km and 60 km), only the first 50 km have been displayed. The amplitudes are arbitrarily normalised, separately for each EOF. The amplitudes of the first EOF are relatively smooth functions of range and separate cold and warm water masses, while those of second and third EOF contain more variability.

Figure 13 presents examples of reconstructed sound-speed profiles, chosen from section S19, cf. Fig. 4c. By considering the first 3 EOFs, good agreement is also found for the profiles within the front (S19: 40 km and 45 km). Figures 14a,b show reconstructed sound speeds of section S19, using the same representation as in Fig. 4c for the measured data. With only the first EOF (Fig. 14a) the front is clearly reproduced, but also additional variability is obtained. Adding the second- and third-order EOFs more structure is introduced. It may be stated that despite some smoothing the reconstructed field agrees well with the measured one. Even better agreement is found for sections more remote from the front (not shown here).

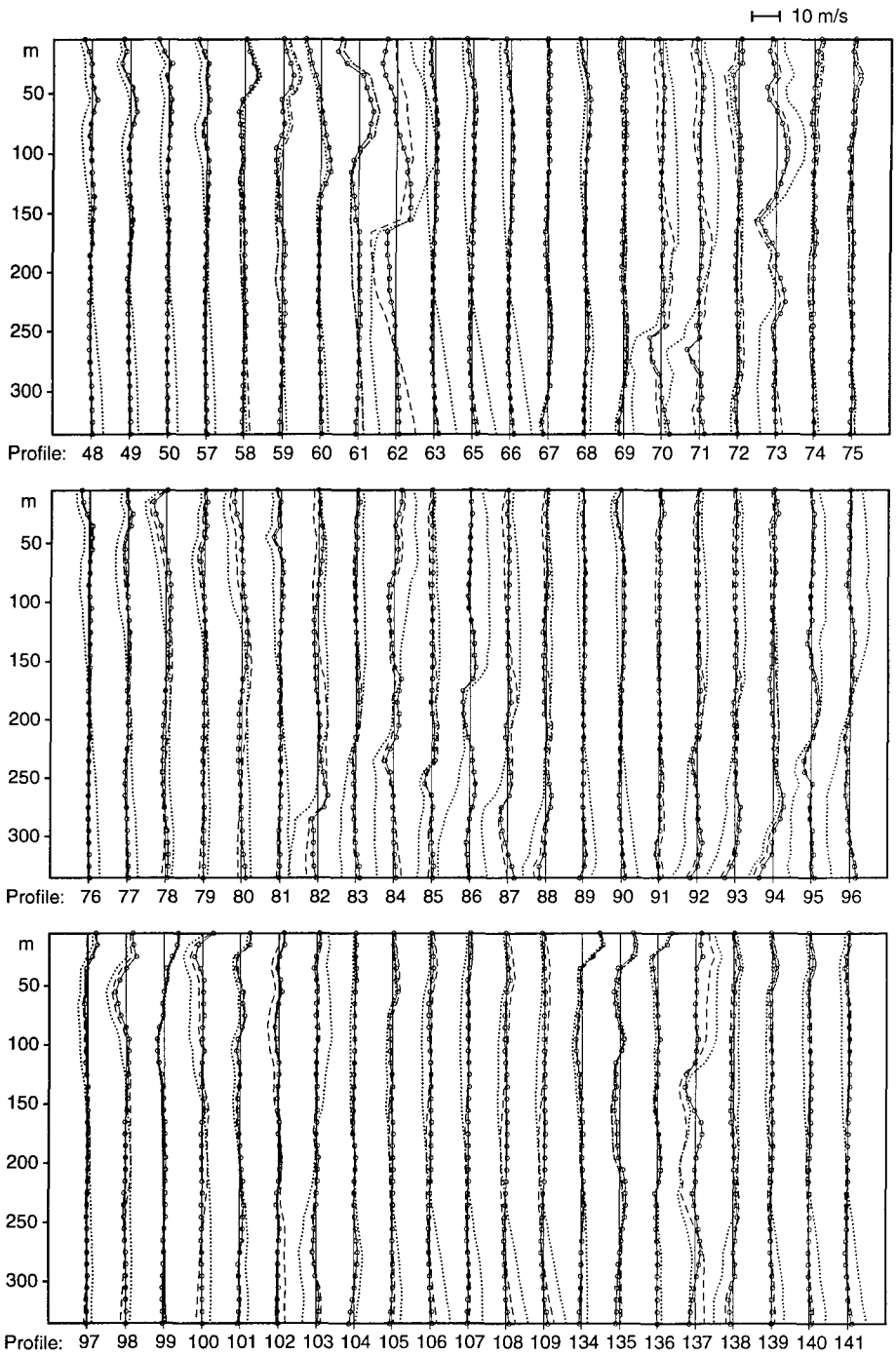

Figure 10 *Difference of measured and reconstructed sound speeds from all profiles of the CTD survey. For reconstruction, first EOF (dotted line), first and second EOF (dashed line) and first through third EOF (solid line with circles) have been used.*

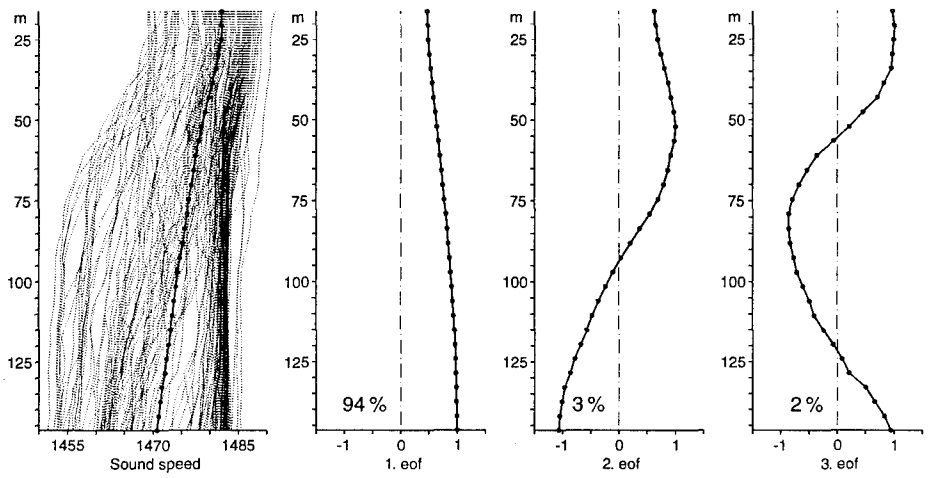

Figure 11 *Vertical sound-speed profiles and the first three EOFs from the thermistor-chain measurements. Each 20th profile from all sections in Fig. 3 is displayed. Dotted lines are the measured profiles, the solid line (marked by circles) is the mean profile (left panel). Sound speeds are in ms^{-1}. The EOF functions are arbitrarily normalised, their percentage amount of variance is indicated.*

3.2. HORIZONTAL CORRELATION LENGTHS

Beside the space series of sound speed, as derived from a satellite image or measured by the thermistor chain, we also investigate the along-track derivatives. These are obtained as central differences,

$$\frac{\mathrm{d}c}{\mathrm{d}r}|_n = \frac{c_{n+1} - c_{n-1}}{2\delta}, \tag{8}$$

where n counts the sample points and δ is the sample distance, i.e., 1 km for the satellite image and 0.5 km for the thermistor-chain data. One method of investigating the variability of random series is by means of their ACF. Considering a zero-mean series p_k of N data points, the ACF may be estimated by

$$\rho_k = \frac{\sigma_k}{\sigma_0} \quad (k = 0, 1, \ldots), \qquad \sigma_k = \frac{1}{N} \sum_{n=1}^{N-k} p_n p_{n+k}. \tag{9}$$

The estimator σ_k of the autocovariance function is only asymptotically unbiased for $k \ll N$, but mimimizes the least-squares errors.

Figure 15 displays ACFs which have been averaged, at four selected depth horizons, over all thermistor-chain sections in Table 1 (except for S10 and S11). The ACF has been computed from series with mean removed (solid lines) and additionally linear (dashed lines) and quadratic trends (dotted lines) removed. For the sound speed itself (c) the ACF depends considerably on the trend removal. Thus, it may be concluded that the process is not homogeneous and that the information on the

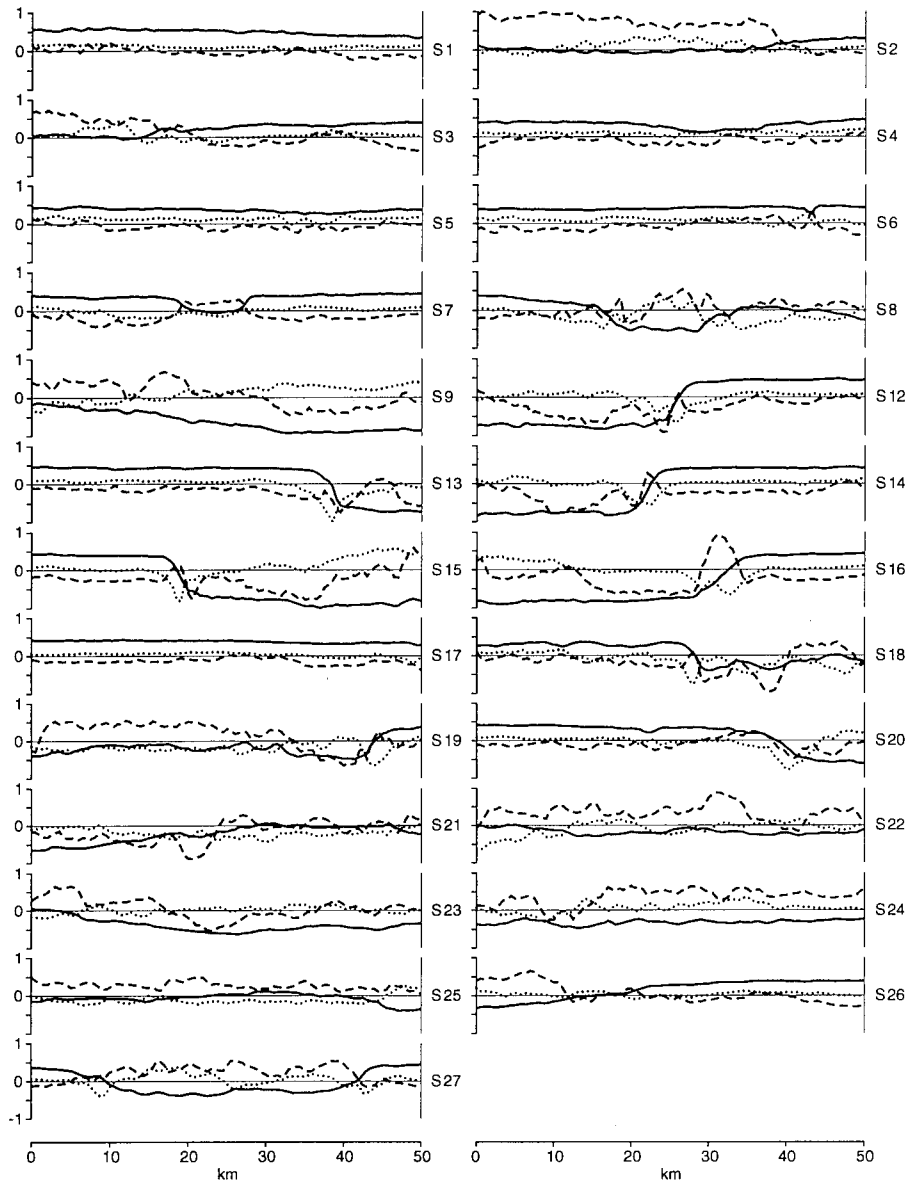

Figure 12 *EOF amplitudes as function of distance for the thermistor-chain sections of Fig. 3. Solid, dashed and dotted lines refer to first, second and third EOF, respectively. The amplitudes are arbitrarily normalised, separately for each EOF.*

random part of the field is distorted. The ACFs of the along-track derivatives (dc/dr) indicate a much steeper decrease and do not depend on trend removal. But also this result has to be considered with caution. The mathematical procedures of taking along-track central differences (8) and computing the ACF (9) interfere with each other and lead to an underestimation of the correlation length. This problem can be avoided by considering across-track derivatives, which are available from satellite

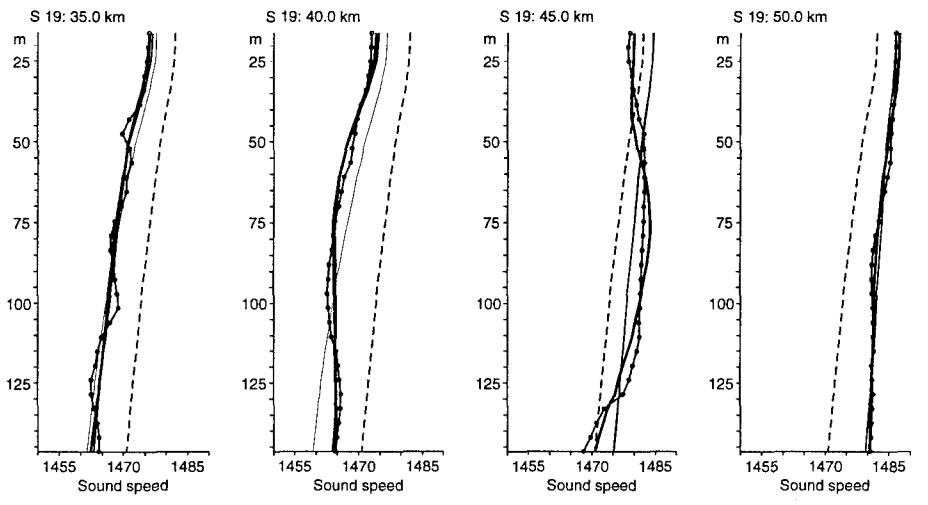

Figure 13 *Reconstruction of sound speed by means of EOFs for four chosen profiles from the thermistor-chain section S19 (cf. Fig. 3). Measured profiles (solid line with circles), mean profile (dashed line), and reconstructed profiles using one, two, or three EOFs (solid lines with increasing thickness) are displayed. Sound speeds are in* ms^{-1}.

images and indeed yield a somewhat larger correlation length, (Essen, 1992) and below.

Mean WVSs are shown in Fig. 16, computed from time series detrended by mean (solid lines), and aditionally by linear (dashed lines) and quadratic trends (dotted lines). The WVSs of the sound speed show a nearly k^{-2} decay, which becomes slightly steeper in the cases of trends subtracted. Except for the very long wavenumbers, there is no difference between the WVSs of space series with only linear or linear and quadratic trend removed. Again, the WVSs of the along-track derivatives have to be considered with caution. They reflect the low-pass filter function introduced by (8). First-order along-track derivatives can also be computed by means of cubic spline interpolation. The respective WVSs are similar to those in Fig. 16 but decay at somewhat higher wavenumbers, i.e., show a more 'white' behaviour.

Mean ACFs (left panel) as well as WVSs (right panel) of the satellite derived sea-surface sound speed are shown in Fig. 17. Averages over 25 south-north orientated sections (y-direction) from Fig. 6 have been taken with a sampling distance of 1 km, which is the resolution of the AVHRR and twice as large as the sampling distance applied to the thermistor-chain data. Again, the ACF of the sound speed itself is strongly influenced by the presence of the front. As already mentioned, the across-track component of the gradient ($\mathrm{d}c/\mathrm{d}x$) indicates a somewhat larger correlation length than that of the along-track component ($\mathrm{d}c/\mathrm{d}y$). As compared to the thermistor-chain data, cf. Fig. 15, the satellite data yield a larger correlation length, which obviously is an artifact of the lower resolution and some smoothing introduced by transforming a distorted satellite image onto an appropriate grid.

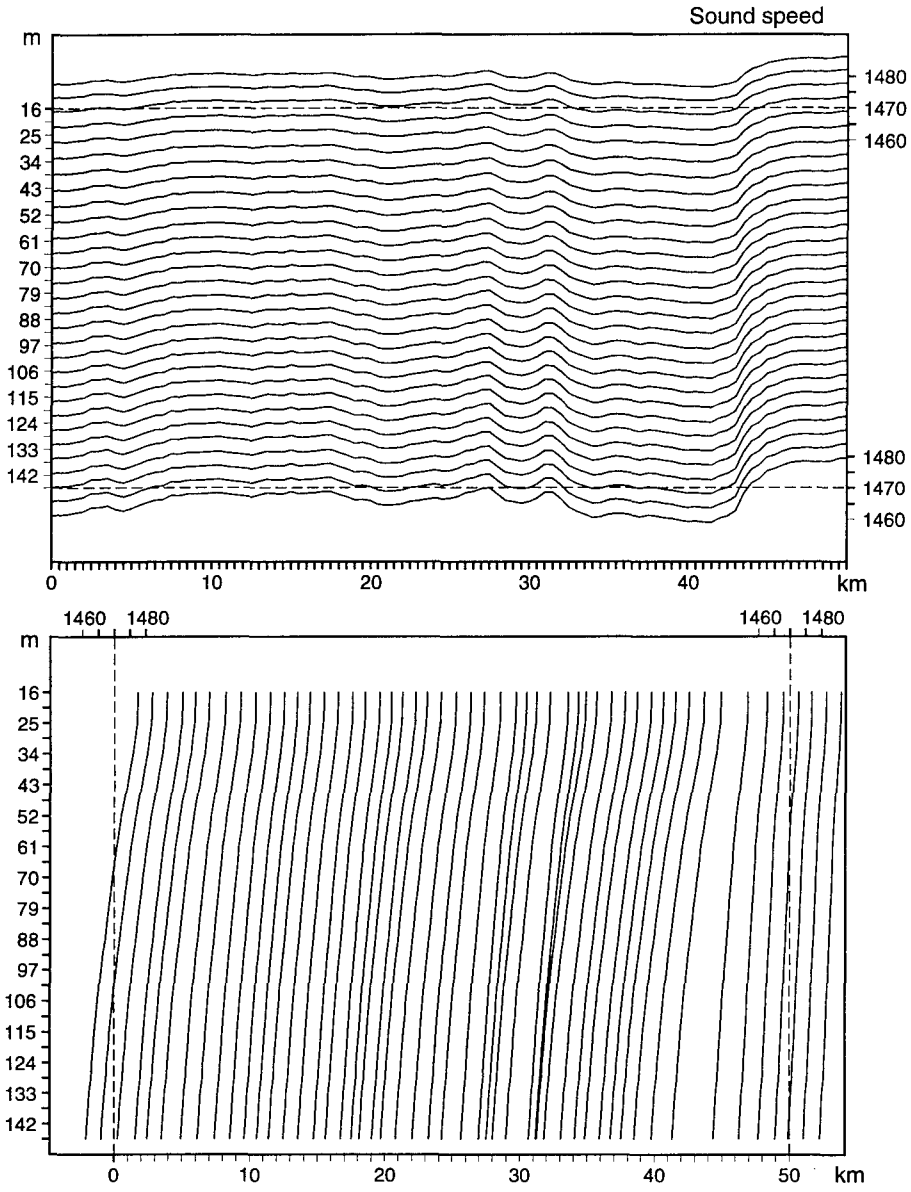

Figure 14a *Reconstruction of sound speeds of the thermistor-chain section S19 by means of the first EOF only. The EOF amplitudes are derived from the measured data. The presentation is the same as in Fig. 4a.*

Despite different sampling rates the scale of the wavenumber axis in Fig. 17 (satellite data) has been chosen in accordance with that of Fig. 16 (thermistor-chain data). The WVSs of both sources show high similarity, both in magnitude and in the wavenumber dependence. Those of the two components of the gradient show different behaviour, obviously due to the deviating filter functions introduced by taking along- and across-track derivatives.

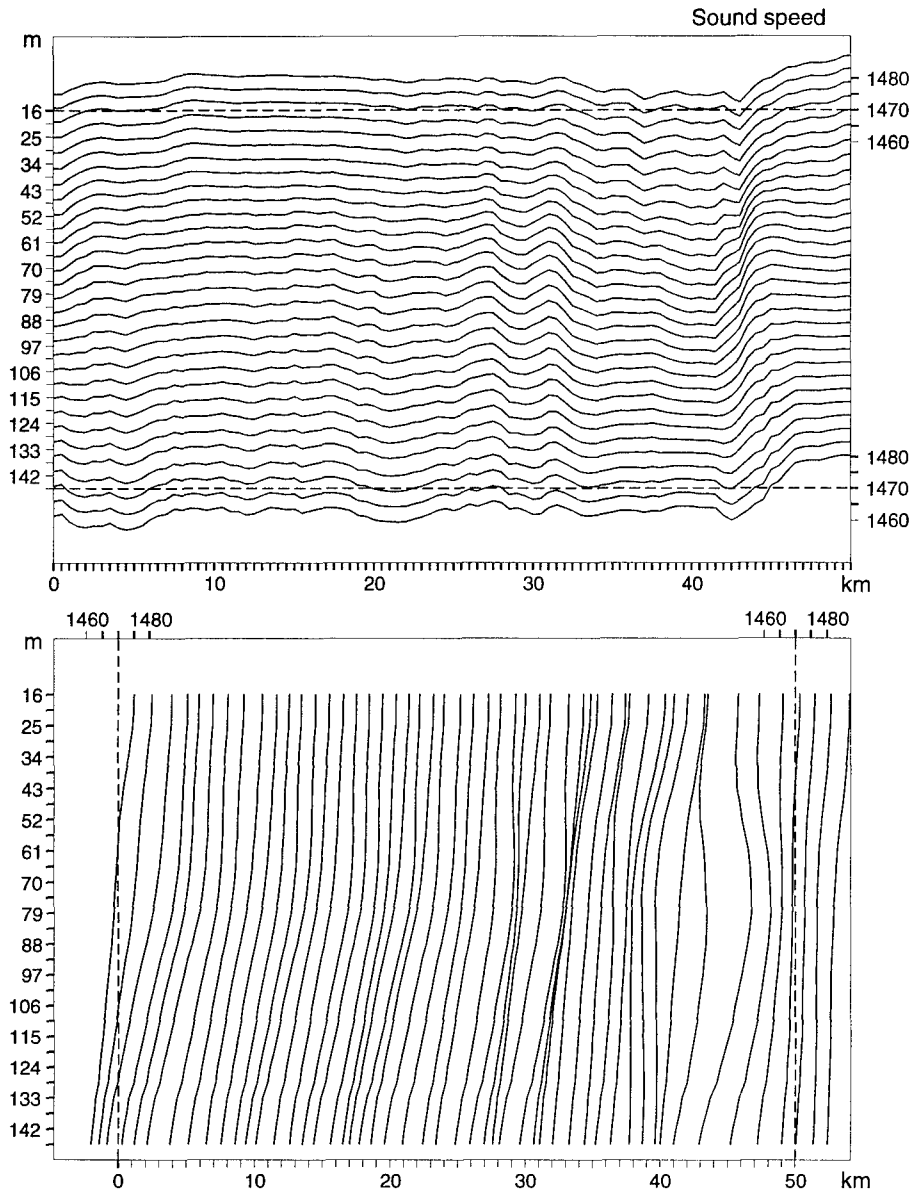

Figure 14b *Reconstruction of sound speeds of the thermistor-chain section S19 by means of the first through third EOF. The EOF amplitudes are derived from the measured data. The presentation is the same as in Fig. 4a.*

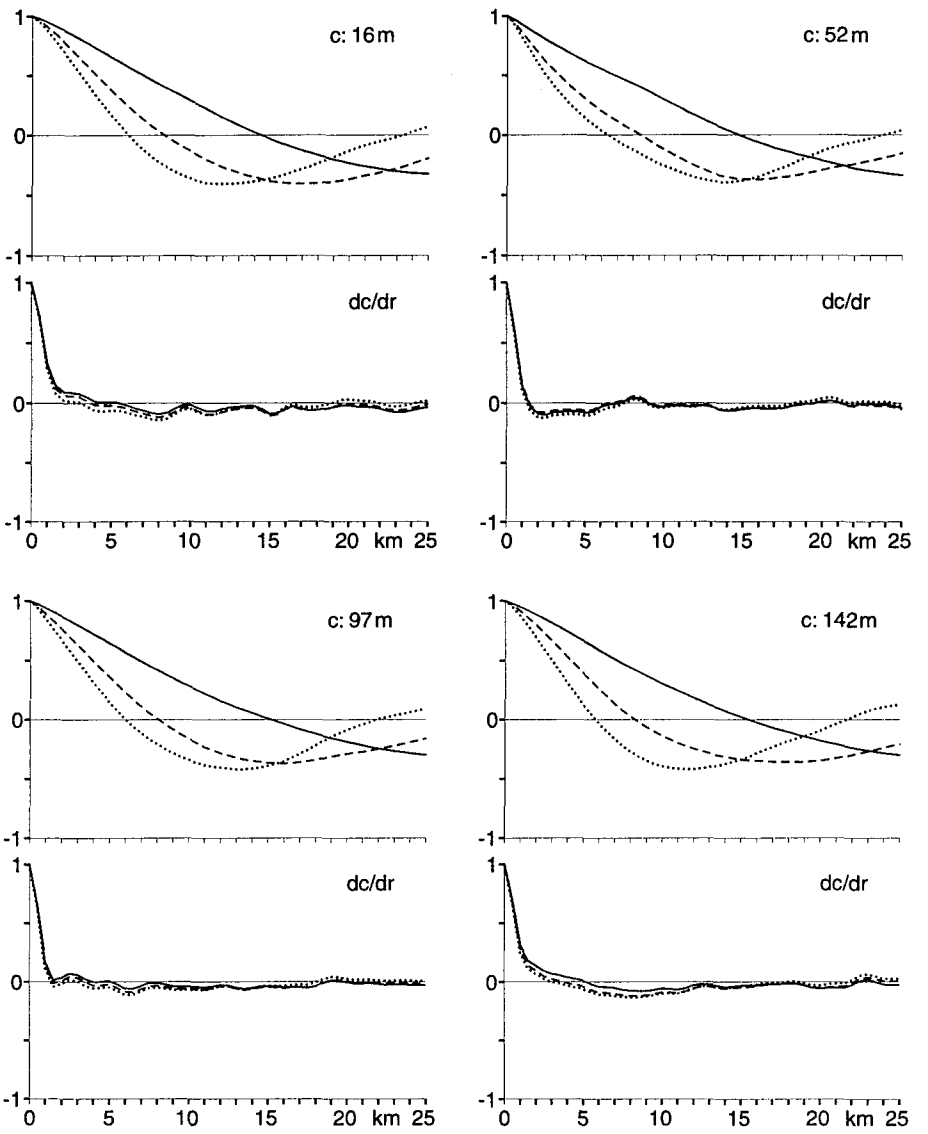

Figure 15 *Mean auto-correlation functions of sound speed (c) and the along-track derivative (dc/dr) from the thermistor-chain data. Averaging, at four selected depths, is performed over all 25 sections available. The three curves refer to removing mean (solid), and additionally linear (dashed) and quadratic (dotted) trends from the space series.*

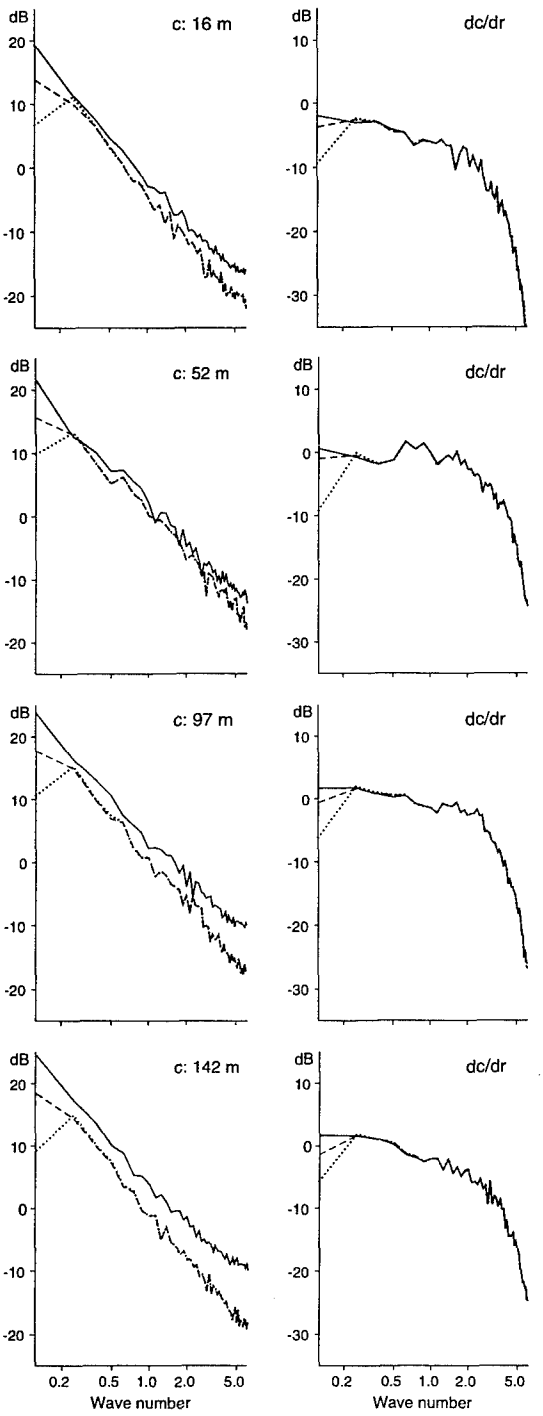

Figure 16 *Mean wavenumber spectra of sound speed (c) and the along-track derivative* (dc/dr) *from the thermistor-chain data. Averaging, at four selected depths, is performed over all 25 sections available. The three curves refer to removing mean (solid), and additionally linear (dashed) and quadratic (dotted) trends from the space series. Wavenumbers are in* km^{-1}.

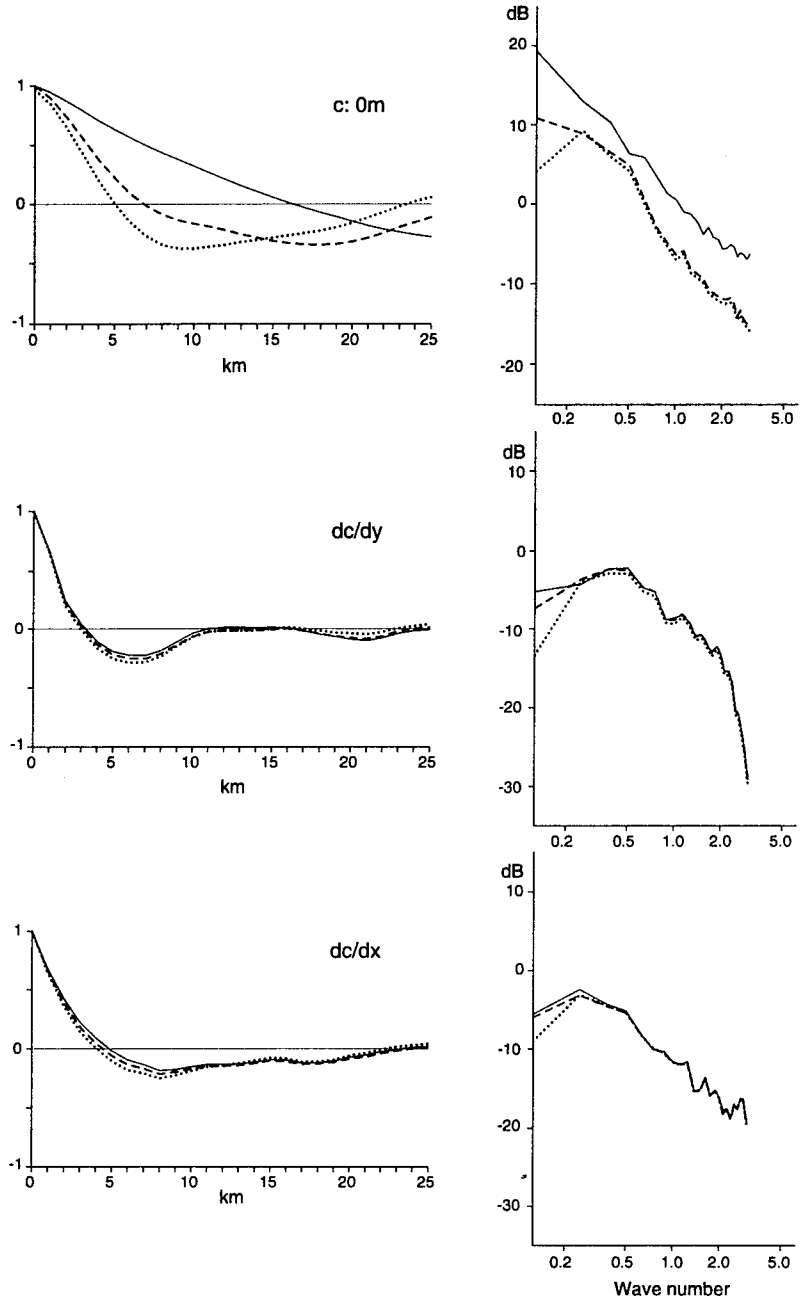

Figure 17 *Mean autocorrelation functions (left panel) and variance spectra (right panel) of sea-surface sound speed, as derived from the satellite SST image Fig. 5. Averaging is performed over 25 north-south sections covering the area of Fig. 6. Both components of the gradient, along- (dc/dy) and across-track (dc/dx) are considered. The three curves refer to removing mean (solid), and additionally linear (dashed) and quadratic (dotted) trends from the space series. Wavenumbers are in* km^{-1}.

4

Determination of subsurface sound speed from satellite data

The investigations presented show that sound-speed profiles in the IFF region may reasonably be described by the first two or three EOFs. Thus, if the mean profile and the eigenfunctions are known from field surveys, the horizontal variability of the three-dimensional sound speed is determined by the respective EOF amplitudes. If these are related to features of the sea surface, the subsurface sound speed could be estimated from satellite data. As mentioned before, a correlation between SST and, at least the first EOF amplitude may be expected. SSTs have been recorded from space for about 15 years by means of infrared radiometry. As these data are available from extended two-dimensional areas, they represent optimal input data. Recent investigations from the Gulf Stream area show that there exists a high correlation between the EOF amplitudes and dynamic height. Dynamic height is a feature of the sea surface and can be recorded by satellite altimetry. These data are available from one-dimensional sections along the satellite track.

We will investigate both the dependence of EOF amplitudes on dynamic height and on SST. For this purpose, we only use the field data. Dynamic height is determined by the integrated density profile, which is not available for the thermistor-chain measurements. Thus, we have to restrict these investigations to the CTD data. SST will be represented by the uppermost measuring level, which is 5 m for the CTD and 16 m for the thermistor-chain data.

4.1. DEPENDENCE OF EOF AMPLITUDES ON DYNAMIC HEIGHT

Cheney (1982) calculated the dynamic height from CTD sections in the western North Atlantic (Gulf Stream/Sargasso Sea) and investigated the relationship between this vertically integrated quantity and thermal parameters, such as the depth of a certain temperature or the temperature at a fixed depth. In all cases he found surprisingly good linear correlations. Also in the Gulf Stream area, deWitt (1987) investigated the statistical relationship between dynamic height at the sea surface and temperatures at standard depths. He first found the correlation between EOF amplitudes of vertical temperature profiles and dynamic height, as computed from CTD sections. Carnes et al. (1990) used these results to determine synthetic temperature profiles from altimeter-derived sea surface heights. Beside the errors arising by constructing temperature profiles from dynamic heights, the presently available accuracy of satellite-measured dynamic heights is a limiting factor to this method.

Carnes et al. (1990) point out that they do not expect to find a unique dependence of subsurface structures on dynamic height as a general feature of the ocean. Variability of dynamic height is of the order of 1 m in the Gulf Stream area and in general considerably less in other regions. Boissier and Bouxin (1991) computed dynamic heights from *in situ* CTD measurements in the northeast Atlantic. On scales of about 100 km they observed a variation in dynamic height of the order of 20 cm. From EOF analysis of vertical sound-speed profiles they found that the first mode accounts for 92% of the variability, and this mode accounts for 96% of the variability of the dynamic height.

The dynamic height d [cm] as a function of a reference depth h [m] with respect to the sea surface is defined by,

$$d(h) = 100\frac{\sigma_r h - \int_0^h \sigma_t(z)\mathrm{d}z}{\sigma_t(0) + 1000}, \tag{10}$$

where $\sigma_r = 27.8\ \mathrm{kg\,m^{-3}}$ is a reference density. In order to quantify the dependence mentioned, a regression analysis is performed by approximating the EOF amplitudes a_n, as defined by (7), through a polynom of order K, of which the coefficients A_k are determined by a least-squares fit,

$$\epsilon^2 = \sum_{n=1}^{N}\left[a_n - (A_0 + \sum_{k=1}^{K} A_k d_n^k)\right]^2 = \text{minimum}, \tag{11}$$

where d_n is the dynamic height at position n. The fit is performed for each significant EOF mode separately. The quality of this approximation may be described by the coefficient,

$$r^2 = \frac{s^2 - \epsilon^2}{s^2}. \tag{12}$$

where s^2 is the variance of the amplitudes a_n. In the case of a linear dependence, i.e., $K = 1$ in (11), r is the correlation coefficient. Figure 18 displays amplitudes of the first three EOFs against dynamic height as computed for the reference depth of 340 m, which is just the depth to which the investigated profiles extend. The order of the regression polynomials was chosen for optimum r^2 as defined by (12). For the first-order EOF amplitudes a linear regression turned out to be adequate. For the second- and third-order EOF amplitudes only fourth-order polynomial yielded optimum fitting. For both first and second-order EOF amplitudes surprisingly high values of r^2 are found. Also the third-order EOF amplitudes show some correlation with dynamic height. In all the cases, the amplitudes are uniquely determined by dynamic height. From these results it seems possible in principle to determine sound-speed profiles from satellite altimetry. Unfortunately, the variation of dynamic height is only of the order of ± 10 cm in the IFF region, i.e., much less than in the Gulf Stream area. The accuracy of present altimeters is also of the order of 10 cm, but some improvement can be expected in the future.

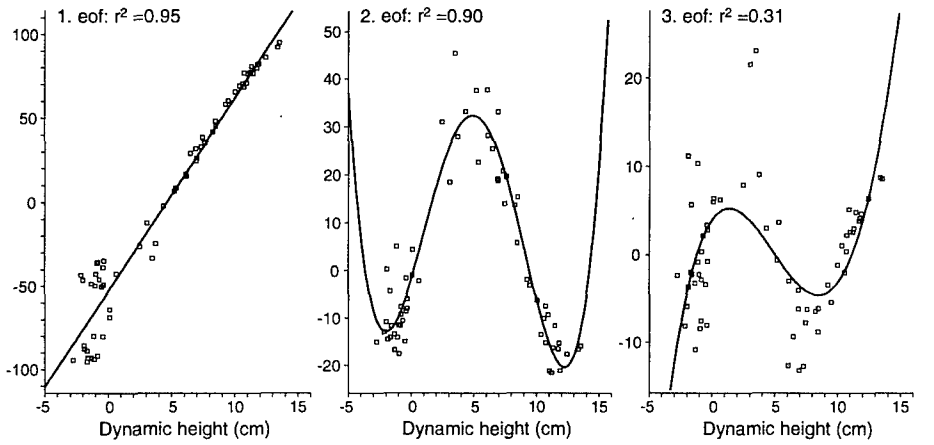

Figure 18 *EOF amplitudes of sound speed vs dynamic height from the CTD survey. Sound-speed profiles extend to 340 m, which is also the reference depth of dynamic height. The regression curve is linear for the first EOF and a fourth-order polynomial for the second and third EOF. See Eq. (12) for the definition of* r^2.

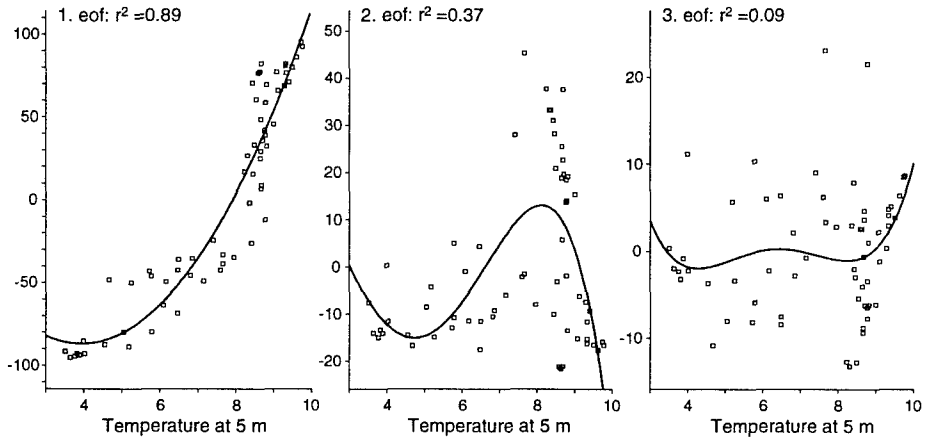

Figure 19 *EOF amplitudes of sound speed vs near-surface temperature (5 m) from the CTD survey. Sound-speed profiles extend to 340 m. Regression curves are polynomials of second-order for the first EOF and fourth-order for the second and third EOF. Temperatures are in* °C. *See Eq. (12) for the definition of* r^2.

4.2. DEPENDENCE OF EOF AMPLITUDES ON SST

Figure 19 presents the same investigation as Fig. 18, but with respect to SST instead of dynamic height. The SSTs are from the uppermost level (5 m) of the CTD data, and the EOF amplitudes are from the sound-speed profiles. The order of the polynomial in (4.2) is $K = 2$ for the first EOF and $K = 4$ for the second and third EOF. Obviously, the correlation is much poorer than for the dynamic height, but still relatively high ($r^2 = 0.89$) for the first EOF.

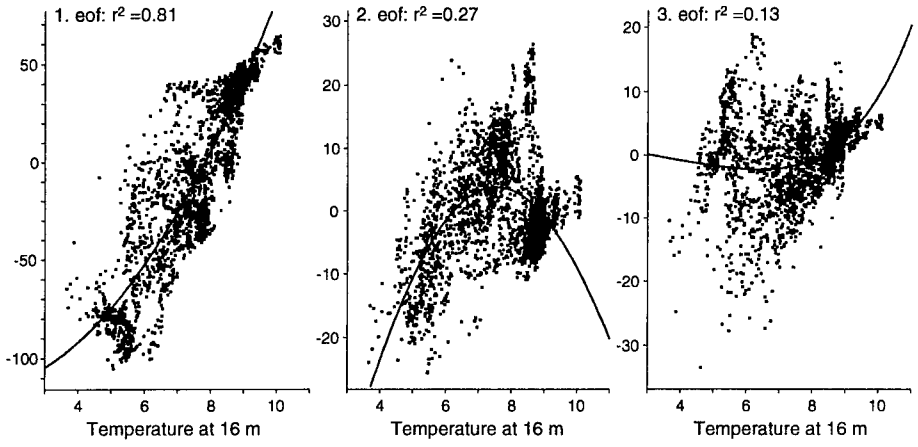

Figure 20 *EOF amplitudes of sound speed vs near-surface temperature (16 m) from the thermistor-chain data. Sound-speed profiles extend to 145 m. Regression curves are polynomials of second-order for the first EOF and fourth-order for the second and third EOF. Temperatures are in* °C. *See Eq. (12) for the definition of* r^2.

Figure 20 contains the same analysis for the thermistor-chain data. Here, the temperature is from 16 m depth, the uppermost measuring level. The sound-speed profiles extend to only 150 m in constrast to 340 m for the CTD data. Nevertheless, the findings regarding the correlation with the EOF amplitudes are about the same as for the CTD data.

Figure 21 compares reconstructed sound-speed profiles, which were obtained by applying the decomposition into EOFs from the CTD survey and the thermistor-chain data. Mean profiles (left panel) are displayed and the profiles reconstructed by means of the first one or two EOFs. For temperatures between 5°C and 9°C, i.e., within the interval observed, the EOF amplitudes were determined from the regression curves in Figs. 19,20. The mean profiles show differences, which may be due in part to the fact that the thermistor-chain measurements were carried out one month later than the CTD survey, but also due to the different locations covered by both experiments. The reconstruction yields good agreement only for 5°C, while for higher SSTs deviations up to 5 ms^{-1} occur. Including the second EOF leads to no improvement, obviously because of the poor correlation of this mode with SST (Figs. 19,20). Further investigations showed (not presented here) that the differences in the reconstructed profiles may not be explained by their deviating lengths.

Referring to Figs. 19,20 it can be stated that only the first-order EOF amplitudes can reliably be estimated from SST. The AVHRR image under investigation is not coincident with the *in situ* experiments. Furthermore it contains brightness temperatures instead of SSTs. In order to account for these discrepencies, mean temperatures have been computed from the frame in the satellite image (4.7°C), the CTD (7.4°C) and the thermistor-chain survey (7.7°C), and the appropriate differences added to the satellite data. With these corrected SSTs first-order EOF amplitudes and in

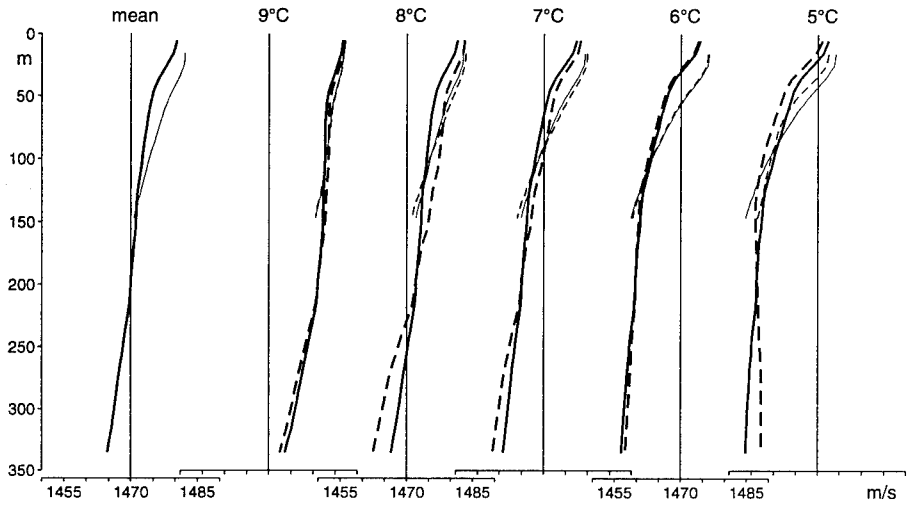

Figure 21 *Comparison of reconstructed sound-speed profiles using the EOFs of the CTD survey (long profiles) and of the thermistor-chain data (short profiles). Mean profiles are displayed (left panel) and profiles reconstructed by means of the first EOF (solid lines) or the first and second EOF (dashed lines). EOF amplitudes are determined from the regression curves in Figs. 19 and 20 for the temperatures indicated.*

turn sound speeds have been determined. For a section from north to south at $x = 40$ km in Fig. 6 the results are presented for the CTD in Fig. 22 and for the thermistor chain in Fig. 23.

Sound-speed profiles in Figs. 22 and 23 extend to different depths. They agree well in the common upper 145 m of the ocean. Comparison with measured data is only possible for the thermistor-chain and only qualitatively, because the measurements and the SST image are not coincident. The sound-speed distribution in Fig. 23 has been deduced from the first EOF only and should thus be compared with Fig. 14a, i.e., the reconstruction of sound speeds by means of the first-order EOF amplitudes of the measured data. Sound-speed profiles in both figures (lower panels) are very similar at both ends of the sections. The variation within the sections is slightly different, the main front is less steep in the satellite than in the thermistor-chain section, but extends over a longer distance (Fig. 6). In addition to the front, Figs. 14a and 23 contain some random-like structures. These however, are considerably smoother than in the original data of Fig. 4c.

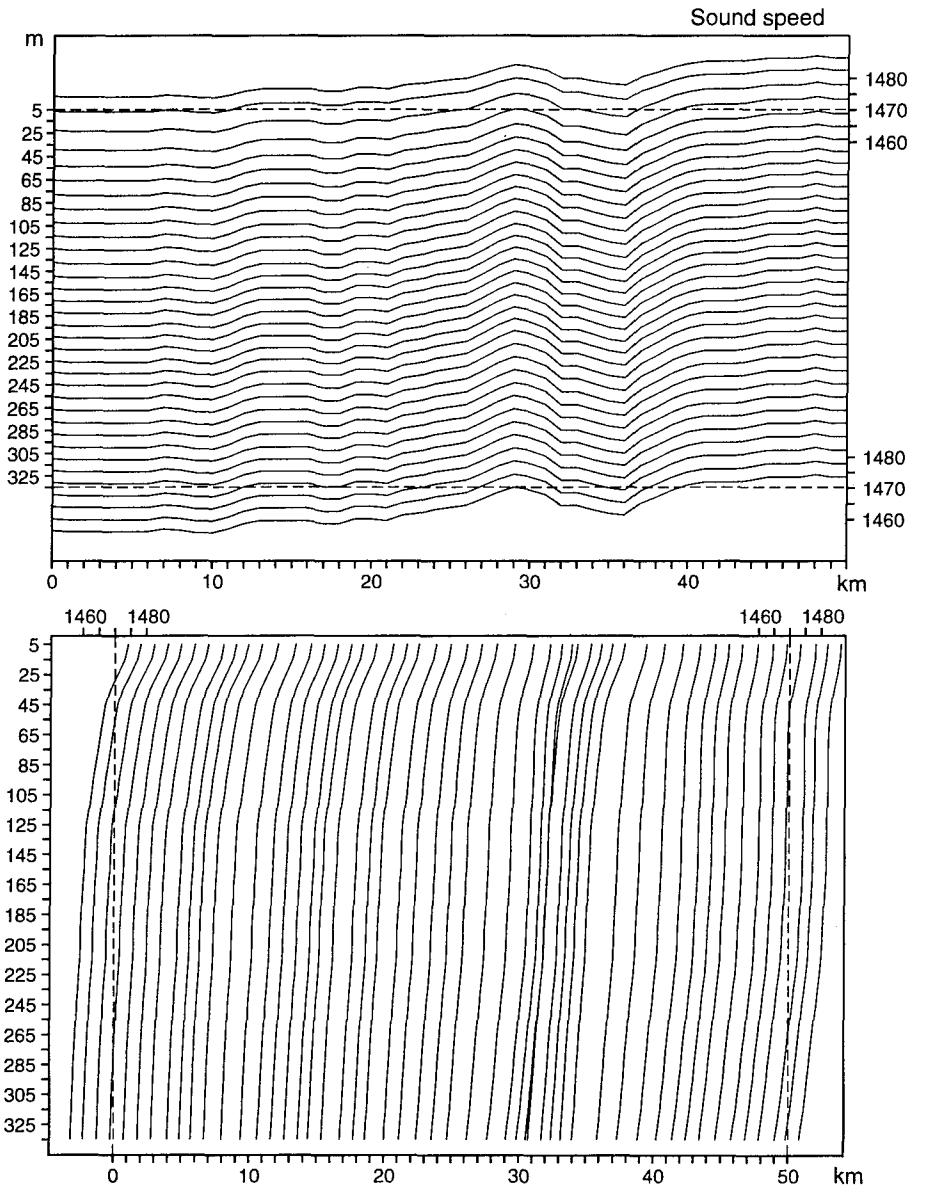

Figure 22 *Sound speeds retrieved from satellite SSTs in the frame of Fig. 5. The section is from north to south at $x = 40$ km in Fig. 6. Only the first EOF of the CTD measurements has been used, with the amplitudes determined via the regression curve in Fig. 19. The AVHRR (channel 4) temperatures have been increased by* 2.7°C. *The presentation is the same as in Fig. 4a.*

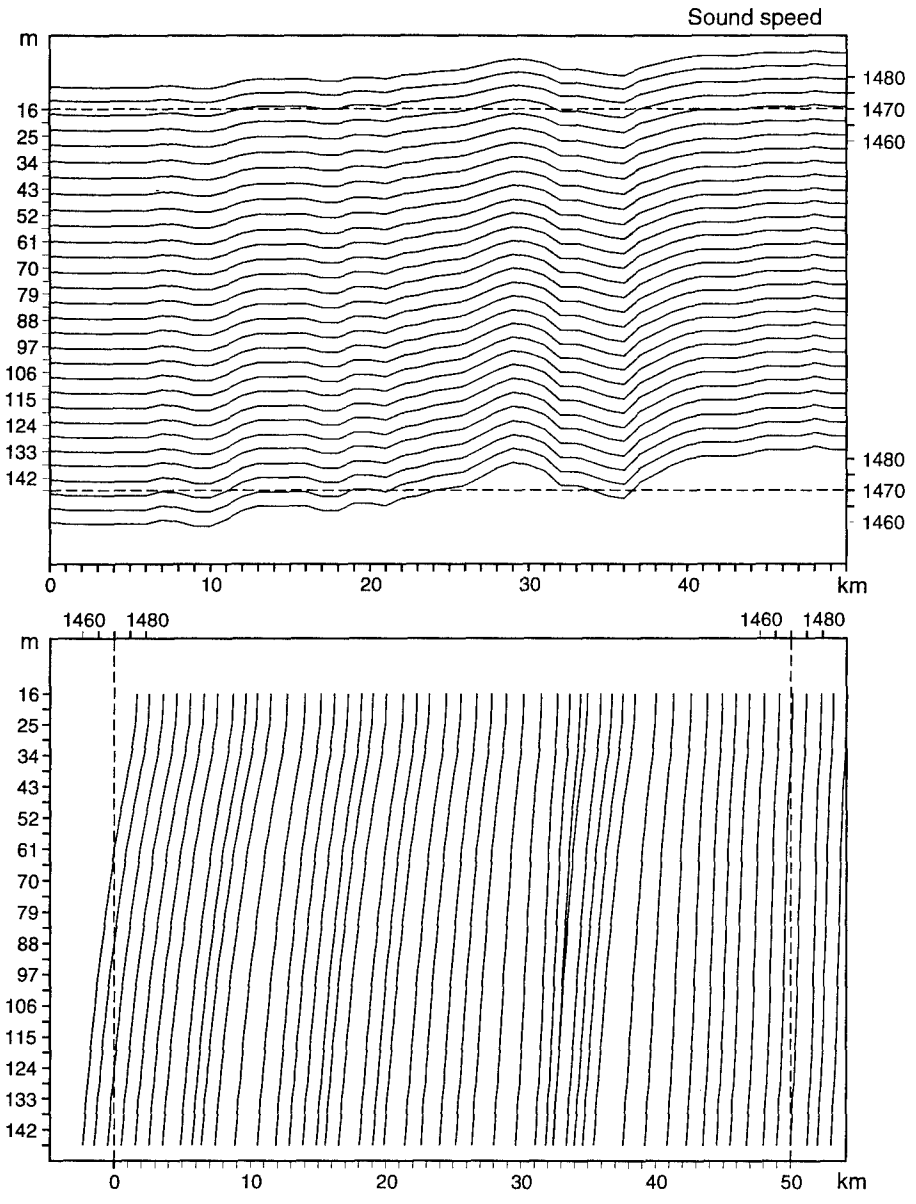

Figure 23 *Sound speeds retrieved from satellite SSTs in the frame of Fig. 5. The section is from north to south at $x = 40$ km in Fig. 6. Only the first EOF of the thermistor-chain measurements has been used, with the amplitudes determined via the regression curve in Fig. 20. The AVHRR (channel 4) temperatures have been increased by* 3.0°C. *The presentation is the same as in Fig. 4a.*

5

Three-dimensional model of sound speed

Sound speed in the IFF region shows a high spatial variability in all three dimensions with horizontal scales of only a few kilometres. For acoustic modelling, sound-speed data of appropriate resolution are necessary but in general not available. To overcome this problem a theoretical model is constructed. For the horizontal variability it is based on the model derived by Essen (1992), which consists of an analytically determined front and random fluctuations represented by a finite moving average process. Instead of applying the model to the sound speed itself, it is used to describe the horizontal variability of the first three EOF amplitudes, which then determine the vertical dependence of sound speed. The model EOF amplitudes $a_n^{(m)}$, as defined by (7), are given by

$$a_n^{(m)} = \alpha_n^{(m)} + \beta_n^{(m)} \qquad (m = 1, 2, 3), \tag{13}$$

where α describes the front and β the random fluctuations, n counts the grid points in the horizontal plain, and m the order of the EOF. We assume that the front can be represented by the first EOF only,

$$\alpha_n^{(1)} = A_0 \tanh A_1(x_n, y_n), \qquad \alpha_n^{(2)} = \alpha_n^{(3)} = 0. \tag{14}$$

As the EOF contributions refer to the mean sound-speed profile, it is assumed that the function A_1 in (14) changes sign across the front and increases in magnitude with distance from the front. The function chosen (tanh) may not be represented by lower order polynomials, as we know is the case with the sound-speed variation at the IFF. The random fluctuations of the EOF amplitudes are derived from a field of normally-distributed white noise $\psi(x_n, y_n)$ by smoothing over a number of adjacent grid points,

$$\beta_n^{(m)} = B^{(m)} \sum_{i,j=-N}^{N} g_{ij} \psi(x_n + i\delta, y_n + j\delta), \tag{15}$$

where δ is the grid distance and $2N$ the order of the finite-moving average process. Following Essen (1992), we use the weights,

$$g_{ij} = \begin{cases} \cos^2(0.5\pi r_{ij}/R), & R_{ij} = \Delta\sqrt{i^2 + j^2} \geq R \\ 0, & R_{ij} = \Delta\sqrt{i^2 + j^2} \geq R \end{cases}, \tag{16}$$

where R is the averaging radius, which by (16) determines N in (15).

Figure 24 displays the gradients of the synthetic sound-speed at the uppermost layer of the EOF functions from the thermistor-chain data (16 m). As in Fig. 6 they are

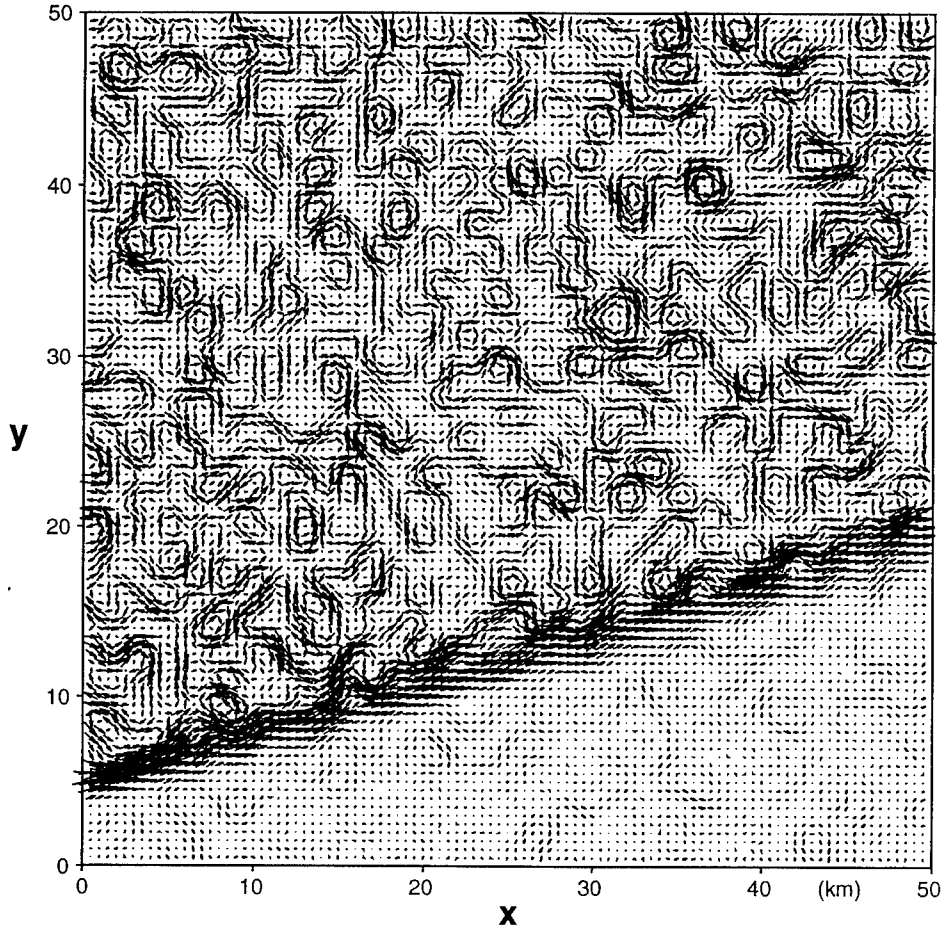

Figure 24 *Horizontal gradients of synthetic sound speeds at the sea surface represented by the orthogonal vectors (4). Coordinates refer to east (x- axis) and north (y-axis). Sound speeds are generated by means of the thermistor-chain EOFs with amplitudes derived from (13–16). Gradients are computed via central differences.*

represented by their orthogonal vectors (4). The position of the front, as well as its slight broadening from west to east is determined by A_1 in (14), the magnitude of change A_0 has been assumed to be independent of position and estimated from the data. Also, the magnitudes of the EOF amplitudes $B^{(m)}$ in (15) do not depend on position and have been determined by looking for optimal agreement with the data. In order to reproduce the vertical correlation visible in Figs. 4a–d, the first EOF has been given a higher weight, $B^{(1)} = 2B^{(2)}$, while those for the second and third EOF are the same, $B^{(2)} = B^{(3)}$. Accounting for the reduced variability south of the front, the respective amplitudes have been reduced to 25% of those north of the front.

Differences between the real and synthetic gradients in Figs. 6 and 24 are obvious. In the synthetic data the front is not bent and the random portion is more homogeneous. Nevertheless, the scales of variability are reproduced. Figure 25 displays

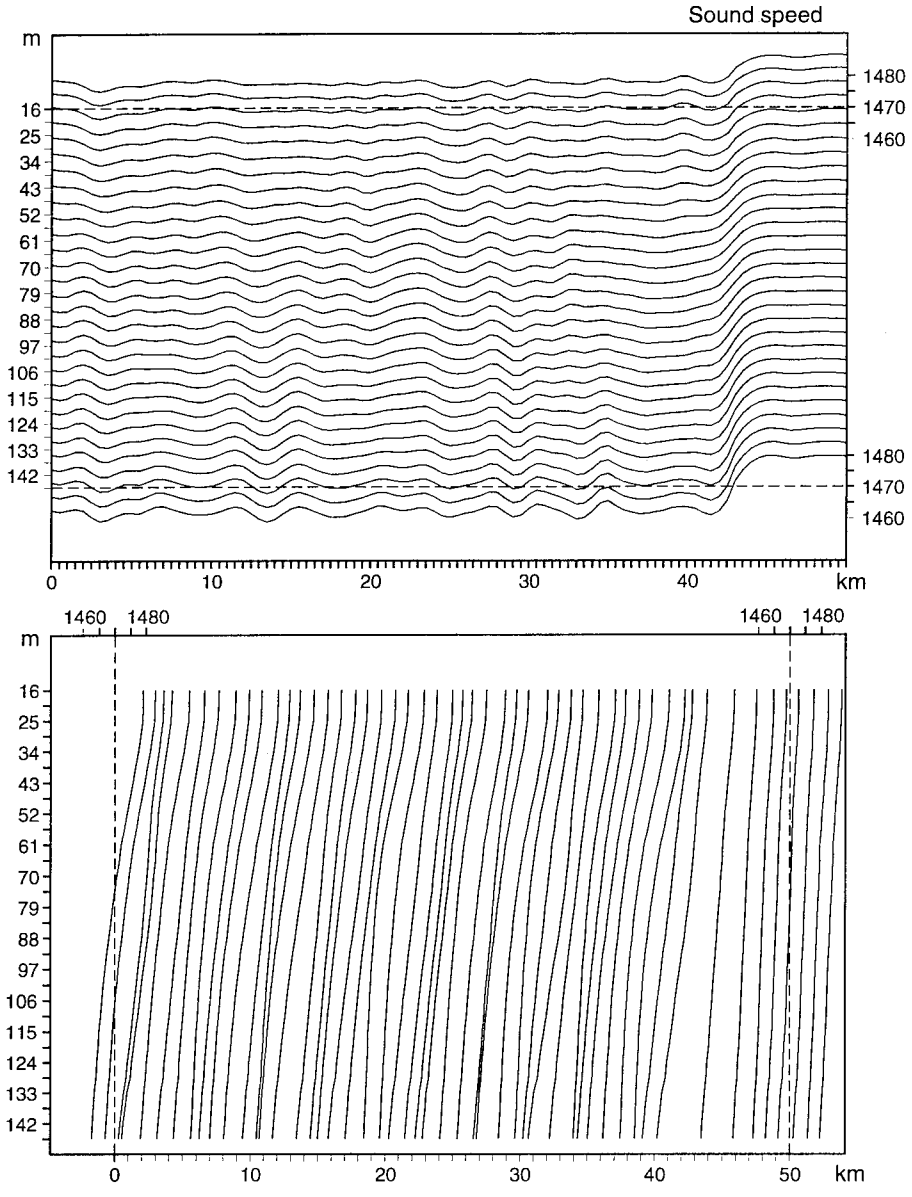

Figure 25 *Sound speeds as generated by synthetic amplitudes of the first three EOFs, using the same method as for Fig. 24. The section crosses the front from south to north at $x = 20$ km in Fig. 24, according to S19 in Fig. 4c. The presentation is the same as in Fig. 4a.*

synthetic sound speeds, the horizontal variability at different depths (upper panel) and each second profile (lower panel). The section crosses the front from north to south at $x = 20$ km in Fig. 24, according to S19 shown in Fig. 4c. Despite some smoothing it may be stated that the main features are well reproduced by the synthetic data. As should be expected, somewhat better agreement is found

with Fig. 14b, i.e., with sound speeds reconstructed by the first three EOFs, with amplitudes retrieved from the data.

Mean ACFs of the synthetic data are presented in Fig. 26 and WVSs in Fig. 27. Both are computed from 25 south-north sections with 2 km spacing through Fig. 24. Excellent agreement is found with the respective statistical descriptors of the data (Figs. 15,16). Experiments with the synthetic data show that both ACF and WVS show only little change if some of the sections do not cross the front, as is the case for the measurements. The first-zero crossing of the sound-speed ACF is determined by the front and decreases to the averaging radius R in (16) without the front.

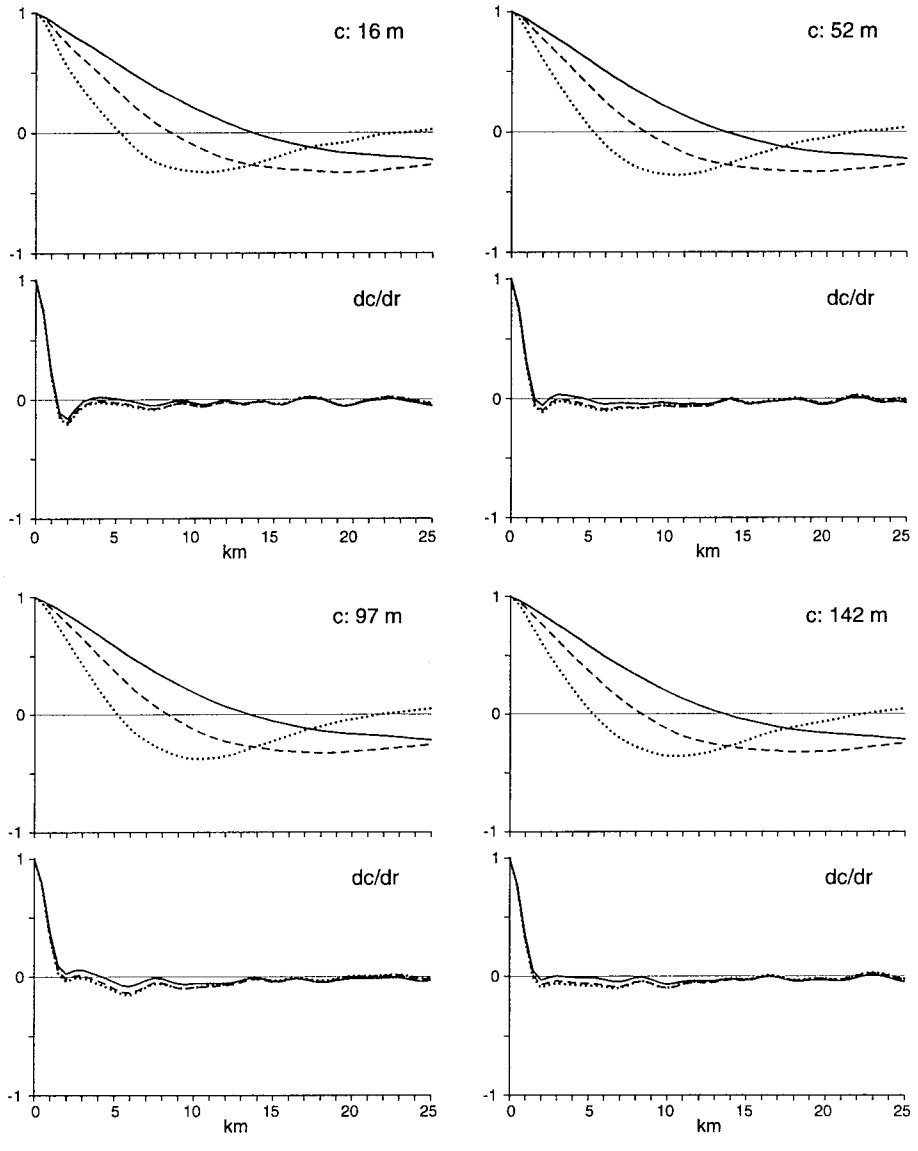

Figure 26 *Mean auto-correlation functions of sound-speed (c) and the along-track derivative* (dc/dr) *from 25 synthetic south-north orientated sections with 2 km spacing (cf. Fig. 24). The three curves refer to removing mean (solid), and additionally linear (dashed) and quadratic (dotted) trends from the space series.*

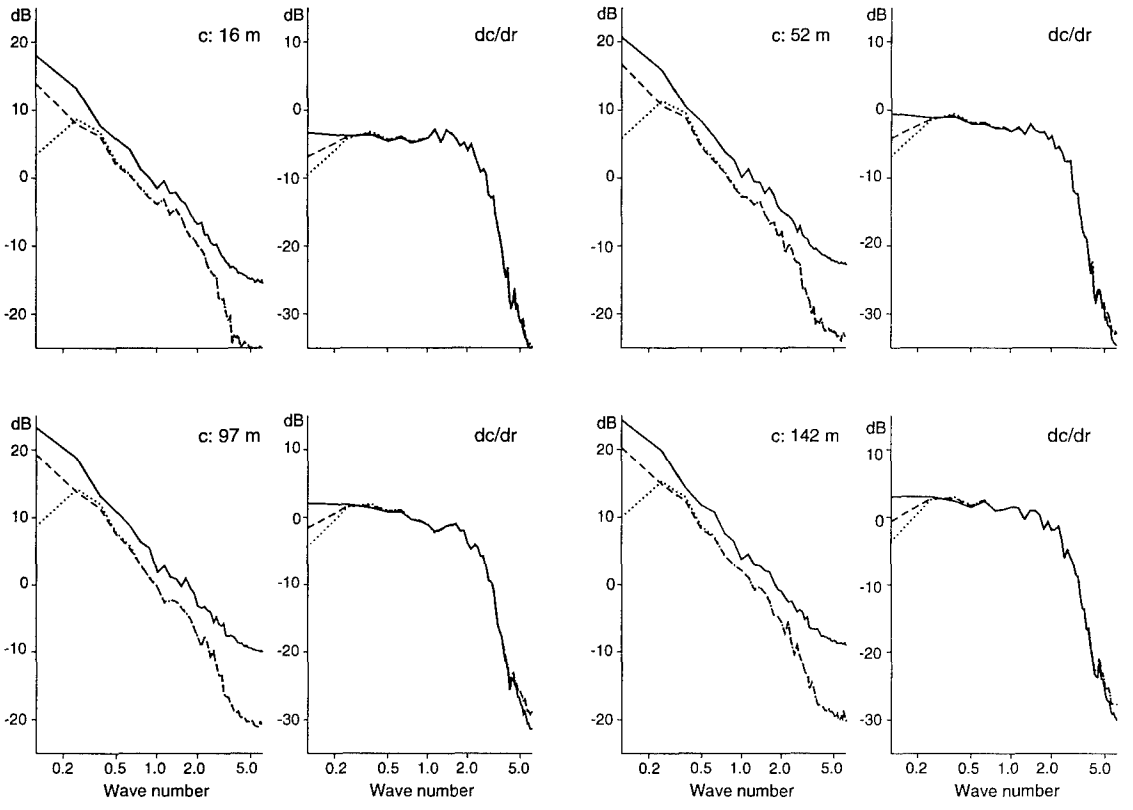

Figure 27 *Mean variance spectra of sound-speed (c) and the along-track derivative (dc/dr) from 25 synthetic south-north orientated sections with 2 km spacing, cf. Fig. 24. The three curves refer to removing mean (solid), and additionally linear (dashed) and quadratic (dotted) trends from the space series. Wavenumbers are in* km^{-1}.

6
Conclusions

CTD data, extending to 340 m depth, and thermistor-chain data, extending to 150 m depth, from the Iceland-Faeroe Frontal region have been analysed with respect to vertical and horizontal variability. It has been shown that vertical sound-speed profiles, deduced from these data, may be decomposed into empirical orthogonal eigenfunctions (EOFs), with the first two EOFs accounting for 97% of the variance. A high correlation of the first-order EOF amplitude exists with sea-surface temperature (SST). If the EOFs are known from field surveys, this correlation allows important features of the subsurface sound-speed structure to be determined from space-borne SST measurements. The sound-speed distribution, as retrieved from satellite-measured SSTs via the first-order EOF amplitudes, mainly accounts for the long-scale variability and smoothes over smaller scales. In addition, a strong vertical correlation is introduced, which is not present in the data. The EOF analysis presented shows that these problems may be overcome by additionally considering second and third-order EOFs. But the respective amplitudes are not correlated with SST and cannot be determined from the satellite images. As for acoustic modelling the short-scale variability may be important, a synthetic model of the three-dimensional sound-speed distribution has been developed, based on the EOF decomposition and the observed horizontal variability. By comparing the thermistor-chain and satellite data it becomes obvious that, due to the limited resolution, the AVHRR overestimates the horizontal scales. For both the thermistor-chain and satellite data it has been found that the horizontal variability is not homogeneous, i.e., may not be uniquely represented by the autocovariance function. For this reason, the synthetic model superimposes a deterministically described front with a random moving average process. In order to account for the vertical variability, the model has been applied to the amplitudes of the first three EOFs, which are known from the field measurements. It has been shown that the model allows the main features of the three-dimensional sound-speed variability in the IFF region to be reproduced.

References

Boissier, C., Bouxin, H. (1991). Radar altimetry and acoustic prediction. *In*: Potter, J., Warn-Varnas, A. (*eds.*): Proceedings of the Workshop on Ocean Variability and Acoustic Propagation, La Spezia, Italy, 4–8 June, 1990. Dordrecht, Kluwer: pp.327-342. [ISBN 0-7923-1079-9]

Brekhovskikh, L.M., Lysanov, Y.P. (1991). Fundamentals of Ocean Acoustics, second edition. Berlin, Springer. [ISBN 3-540-52796-2]

Carnes, M.R., Mitchell, J.L, deWitt, P.W. (1990). Synthetic temperature profiles derived from Geosat altimetry: Comparison with air-dropped expendable bathythermograph profiles. *Journal of Geophysical Research*, **95**, 17979–17992.

Cheney, R.E. (1982). Comparison data for SEASAT altimetry in the western North Atlantic. *Journal of Geophysical Research*, **87**, 3247-3253.

deWitt, P.W. (1987). Modal decomposition of the monthly Gulf Stream/Kuroshio temperature fields, NOO–TR–298. Stennis Space Center, MS, Naval Oceanographic Office. [AD B 118 349]

Essen, H.-H. (1992). Horizontal scales of sound velocity at the Iceland-Faeroe Front as deduced from satellite-measured sea-surface temperatures, SACLANTCEN SR-200. La Spezia, Italy, NATO SACLANT Undersea Research Centre. [AD B 171 011]

Hopkins,T.S. (1988). The GIN Sea, review of physical oceanography and literature from 1972, SACLANTCEN SR-124. La Spezia, Italy, NATO SACLANT Undersea Research Centre. [AD B 144 455] *Also: Earth Science Reviews*, **30**, 1991:175-318.

Minnett, P.J. (1991). Consequences of sea-surface temperature variability on the validation and applications of satellite measurements. *Journal of Geophysical Research*, **96**, 18475–18489.

Sellschopp, J. (1987). Towed thermistor chain data collected during the cruise 'NORDMEER 1987', FWG-Bericht 1987-4. Kiel, Forschungsanstalt der Bundeswehr für Wasserschall- und Geophysik.

Document Data Sheet

NATO UNCLASSIFIED

Security Classification		Project No.
NATO UNCLASSIFIED		23
Document Serial No.	**Date of Issue**	**Total Pages**
SR-226	November 1994	46 pp.

Author(s)

H.-H. Essen and J. Sellschopp

Title

Three-dimensional distribution of sound speed in the Iceland–Faeroe area, retrieved from a CTD survey, thermistor-chain measurements and satellite SST imagery

Abstract

The three-dimensional variability of sound speed in the Iceland-Faeroe Frontal (IFF) region is investigated. Emphasis is put on the question, to what extend subsurface sound speed may be determined from space- borne remote sensing. Data from different sources are used: CTD survey and thermistor-chain measurements as ground truth and satellite infrared imagery. Most of the data are temperatures which, for the area under consideration, quite accurately determine the sound speed. From the subsurface data it is shown that the vertical sound-speed profiles can be decomposed into empirical orthogonal eigenfunctions (EOFs), with the first two already accounting for 97% of the variance. High correlation of the first- and second-order EOF amplitudes is found with sea-surface dynamic height, and for the first-order EOF amplitude with sea-surface temperature (SST). The latter relation is used successfully to determine subsurface sound speeds from satellite-measured SSTs. Due to the resolution of the satellite data, horizontal scales are overestimated, and due to the availability of only the first-order EOF amplitude for the construction of sound-speed profiles, a too high vertical correlation is introduced. To overcome these problems, for the purpose of acoustic modelling, a theoretical three-dimensional sound-speed model is developed, based on the EOF decomposition. The EOF amplitudes contain the analytically described front and random portions represented by a finite moving average process.

Keywords

CTD survey, Iceland-Faeroe Front, satellite infrared imagery, sound-speed variability, thermistor chain

Issuing Organization

North Atlantic Treaty Organization
SACLANT Undersea Research Centre
Viale San Bartolomeo 400, 19138 La Spezia, Italy

tel: 0187 540 111
fax: 0187 524 600
telex: 271148 SACENT I

[From N. America: SACLANTCEN CMR-426 (New York) APO AE 09613]

NATO UNCLASSIFIED

Initial Distribution for SR-226

Ministries of Defence	
DND Canada	10
CHOD Denmark	8
MOD France	8
MOD Germany	15
MOD Greece	11
MOD Italy	10
MOD Netherlands	12
CHOD Norway	10
MOD Portugal	5
MOD Spain	2
MOD Turkey	5
MOD UK	20
SECDEF US	54
NATO Authorities	
NAMILCOM	2
SACLANT	3
CINCIBERLANT	1
COMSUBACLANT	1
COMNAVSOUTH	1
SCNR for SACLANTCEN	
SCNR Belgium	1
SCNR Canada	1
SCNR Denmark	1
SCNR Germany	1
SCNR Greece	1
SCNR Italy	1
SCNR Netherlands	1
SCNR Norway	1
SCNR Portugal	1
SCNR Spain	1
SCNR Turkey	1
SCNR UK	1
SCNR US	2
French Delegate	1
SECGEN Rep. SCNR	1
NAMILCOM Rep. SCNR	1
National Liaison Officers	
NLO Belgium	1
NLO Canada	1
NLO Denmark	1
NLO Germany	1
NLO Italy	1
NLO Netherlands	1
NLO UK	1
NLO US	1
Total external distribution	203
SACLANTCEN Library	22
Total number of copies	225